Reconstructing Paleofluid Circulation at the Hercynian Basement/Mesozoic Sedimentary Cover Interface in the Upper Rhine Graben

Chrystel Dezayes, Catherine Lerouge

Hindawi
Geofluids
Volume 2019, Article ID 4849860, 30 pages
https://doi.org/10.1155/2019/4849860

Research Article

Reconstructing Paleofluid Circulation at the Hercynian Basement/Mesozoic Sedimentary Cover Interface in the Upper Rhine Graben

Chrystel Dezayes and Catherine Lerouge

BRGM, 3, avenue Claude Guillemin, BP36009, 45060 Orléans Cedex 2, France

Correspondence should be addressed to Chrystel Dezayes; c.dezayes@brgm.fr

Received 24 April 2018; Revised 10 October 2018; Accepted 26 November 2018; Published 6 March 2019

Academic Editor: Domenico Montanari

In this paper, we focus on paleocirculation at the Hercynian basement/sedimentary cover interface in the tectonic environment of the Upper Rhine graben. The goal is to increase our understanding of the behavior of the fracture-fault network and the origin of the hydrothermal fluids. We studied orientations, mineral fillings, and fluid origins of fractures that crosscut the Hercynian granitic basement and the Permo-Triassic formations in relation to the major tectonic events. Because the Mesozoic formations and the Hercynian basement on the graben flanks and inside the graben do not have the same evolution after uplift, our study includes 20 outcrops on both graben flanks and cores of the Soultz-sous-Forêts geothermal wells located inside the graben. The Hercynian granitic basement and Permo-Triassic formations were affected by several brittle phases associated with fluid circulation pulses related to graben formation during the Tertiary. We distinguished at least four stages: (1) reactivation of Hercynian structures associated with pre-rift tectonics during the early Eocene and descending meteoric waters, characterized by shearing/cataclasis textures and precipitation of illite and microquartz; (2) initiation of convective circulation of deep hot brines mixed with descending meteoric waters at the Hercynian basement/sedimentary cover interface during this first stage of Eocene rifting, characterized by dolomite and barite fillings in reactivated Hercynian fractures; (3) N-S tension fractures associated with rift tectonics just prior to uplift of the graben shoulders during Oligocene extension and descending meteoric waters, characterized by cataclastic textures and precipitation of quartz, illite, hematite, and barite; and (4) current convective circulation of deep hot brines mixed with descending meteoric waters at the Hercynian basement/sedimentary cover interface, characterized by calcite and barite fillings within the graben. This convective circulation is today present in deep geothermal wells in the western part of the Rhine graben.

1. Introduction

In studying geothermal systems, knowledge of fluid pathways at depth is critical for improving exploration for future resources while reducing geological risk.

Fluid migration through the crust depends to a great extent on the permeability and porosity of the rocks being crosscut [1]. These two parameters represent the rock's capacity to transmit fluid. Permeability and porosity depend on the initial rock type (sediments, magmatic rocks, and metamorphic rocks) [2] and geological processes that the rock has undergone during its history. These include fluid/rock interactions (low/high fluid/rock ratios), deformation (ductile/brittle), and pressure/temperature changes (e.g., diagenesis, metamorphism, hydrothermal alteration, and weathering). In tectonically and/or thermally stable environments, permeability may reduce drastically at depth and fluid/rock interactions are likewise reduced. In more active environments, geological evidence from several studies shows that hydrological systems operate at different scales and at all depths of the continental crust [1].

Hydrogeologists and geologists want to understand the nature, origin, and role of fluids in such fundamental geological processes as hydrothermal systems [3], deep geothermal

systems [4, 5], ore deposition [6, 7], hydrocarbon maturation, migration and entrapment [8], seismicity [9], and metamorphism [10–12]. In sedimentary rocks, fluid pathways include connected rock porosity and lithological changes. Burial diagenesis may significantly modify rock mineralogy and porosity. Fluid circulation in massive magmatic and metamorphic rock at depth usually occurs through fracture and fault networks at different scales [13, 14], and the porosity is predominantly fracture porosity depending on the geometry and kinematics of the fault-fracture network [15, 16]. Intense fluid/rock interactions significantly modify the mineralogy (hydrothermal alteration of the host rock, mineralization precipitated in fractures) and matrix porosity (primary) as well of fracture porosity (secondary) [17].

In active environments, rift systems such as the Rhine graben act as major conduits for both magma and hydrothermal fluids [18, 19]. The Rhine graben is part of the European Mid-Continental Rift System [20] (Figure 1(a)), which for several decades has been a target for the development of deep geothermal exploitation in the granitic basement [21]. The crust below the Rhine graben is relatively thin, and the mantle probably underlies the crust at proximal depths based on ^{3}He anomalies [22], and therefore, the heat flow is high [23]. In contrast, at the local scale a well-developed fracture network favours the development of hydrothermal cells and promotes the vertical advection of fluids and heat [16, 24]. Deep geothermal projects seek to exploit hot water at great depth (around 4 to 6 km), hosted in quasi-impermeable granite and deep sediments and where hot fluids circulate primarily within the fault-fracture network. For these reasons, deep geothermal projects are risky and require good characterization of the geometry of the fault-fracture network and its permeability and of the regional fluid flow to optimize well siting and to locate geothermal fluids at depth.

The structural, mineralogical, and petrophysical characterizations of the granitic basement within the graben remain accessible only by drilling. Some of this information can also be obtained by studying rock analogues on the graben flanks as an exhumed geothermal area affected by circulation of geothermal fluids (i.e., [25]). The uplifted flanks affect the present-day regional fluid flow [26], where the higher topography creates a hydrodynamic gradient that drives water downward into sediment-hosted aquifers [22, 27, 28]. Understanding the thermal history of the graben flanks also helps us understand the thermal regime within the graben [23, 29–31].

In this paper, we focus on the relationships between mineral filling, fluid circulation, and tectonic history in the Upper Rhine graben to characterize the hydraulic behavior of the fracture-fault network and the origin of hydrothermal fluids at the Permo-Triassic sedimentary cover/Hercynian basement interface.

The Hercynian basement and Mesozoic formations on the graben flanks have the same pre-rift history as those inside the graben but are not expected to have the same Tertiary history after the uplift subsequent to the graben collapse that has occurred since the Oligocene. Moreover, these outcropping basement and Mesozoic formations have undergone recent weathering, whereas the deep sandstones and granite have not been affected. To discriminate between the Hercynian and the graben-opening brittle tectonics, we revisited the fractures in the EPS1 well located at the Soultz-sous-Forêts EGS (enhanced geothermal system) site within the Rhine graben and compared them with fracture analysis on surface Paleozoic and Permo-Triassic outcrops and quarries at 20 different sites in the Vosges and Black Forest massifs. In the field, we described mineralized fractures, measured their orientations, and collected samples to provide details on mineralogy and microtextures (Figure 2).

2. Geological Background

2.1. Rhine Graben Setting. The Upper Rhine graben is a Cenozoic graben belonging to the west European rift system (Figure 1(a)) [20], which is well known as a result of numerous studies for petroleum and mining exploration (wells, geophysical surveys, etc.). The graben, oriented roughly N20°E (Figure 1(b)), is filled with Tertiary and Quaternary sediments with minor volcanic activity. The Tertiary cover (500 to 1000 m thick) overlies Jurassic (about 150 m thick) and Triassic (about 700 m thick) sediments and the Paleozoic crystalline basement (Figures 1(c) and 1(d)).

In this paper, we focus on the structural inheritance of the Hercynian basement and the evolution of the fracture network through the most recent Cenozoic phases. The crystalline basement is characterized by three major terranes: the Rheno-Hercynian, the Saxo-Thuringian, and the Moldanubian zones, which exhibit major lithological differences [32, 33]. These terranes were accreted during the main tectonic phases of the Carboniferous (Sudete phase) and Permian (Saalian phase) along NE-SW sutures (Figure 1(b)) [34–36]. In the Vosges [37] and along the western graben border [38], these tectonic phases caused brittle tectonics with primary fracture sets oriented N45°E, N135°E, and N-S for the Carboniferous phase and N60°E to N90°E and N120°E for the Permian phase (Figure 3).

The Hercynian terranes were intruded by Carboniferous granitoids during the Visean (-340 Ma) and Permian (-270 Ma). These granitoids exhibit a broad petrological and geochemical diversity related to a variety of deep active magmatic sources and various petrogenetic mechanisms [39, 40]. The granitoids were emplaced along a NE to NNE direction related to primary weakness zones such as collisional or shear zones (Figure 1(b)).

At the end of the Hercynian orogeny, collapse of the chain led to local extension-related basin subsidence and rhyolitic volcanic activity during the Late Carboniferous-Early Permian [41]. These fault-controlled basins are oriented in a NW direction in the Vosges and the Black Forest massifs (Figure 1(b)).

After a long period of sedimentation during the Triassic and Jurassic characterized by deposition of clastic and carbonate sediments, the area was uplifted starting in the late Jurassic and continuing until the early Eocene (Figure 3). Rifting occurred during the Tertiary, between the end of the Eocene and the beginning Miocene [42]. The inherited Hercynian NE-SW- and NNE-SSW-striking crustal weaknesses were reactivated during the formation of the Rhine

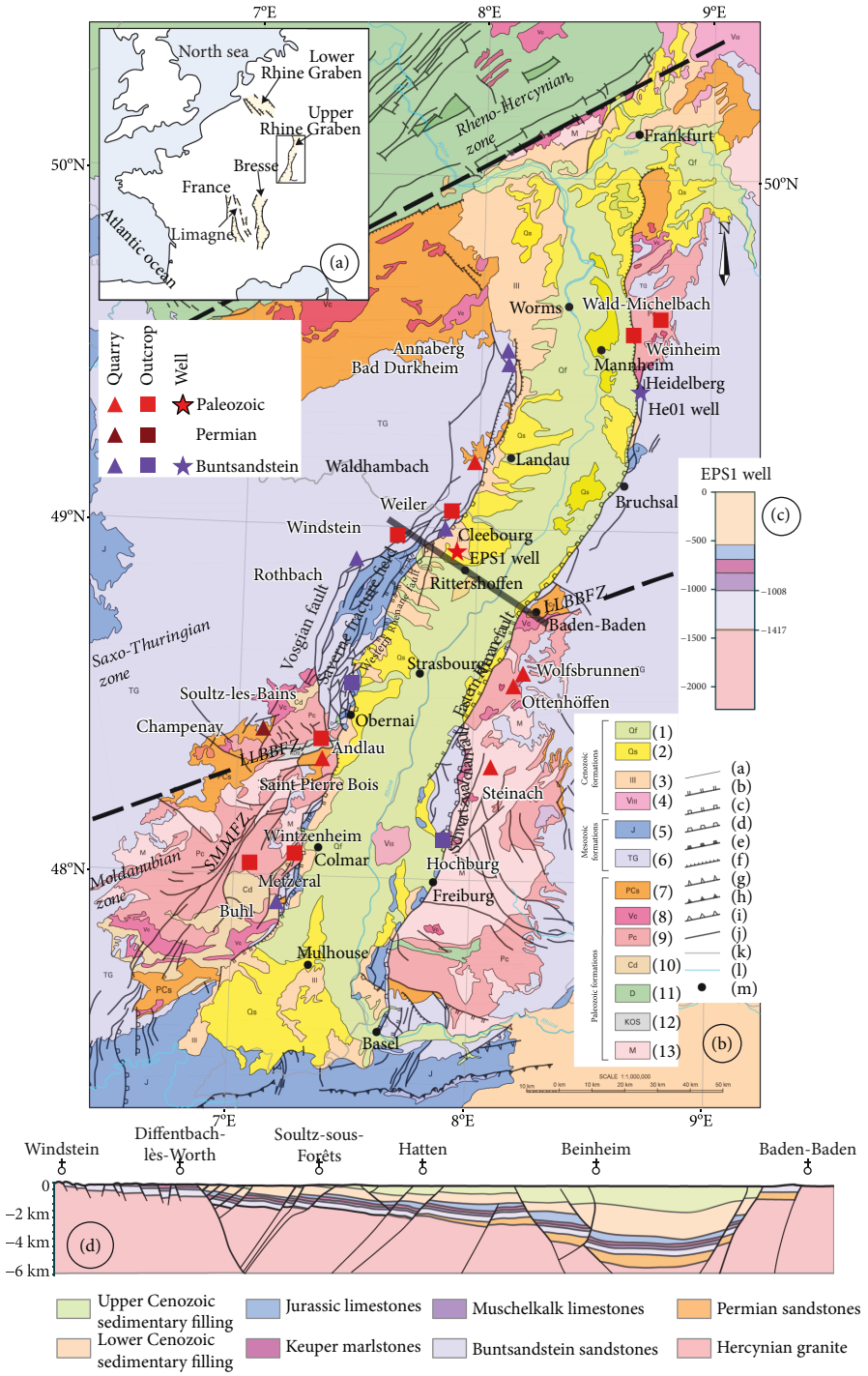

FIGURE 1: Geological setting. (a) Location of the Rhine graben in Western Europe. (b) Geological map from [114] showing location of sampling sites, quarries, outcrops, and wells. (1) Quaternary fluvial deposits; (2) Quaternary loess, eolian deposits; (3) Tertiary marine and lacustrine limestones, marls, evaporites; (4) Tertiary basalt; (5) Jurassic limestones; (6) Triassic sandstones, marly limestones, and anhydrite (German Triassic); (7) Permian red sandstones; (8) Carboniferous volcanism; (9) Carboniferous granites; (10) Dinantian conglomerate; (11) Ordovician-Silurian limestones and continental altered rocks; (12) Ordo-Silurian-Cambrian clay and argillaceous sandstones; (13) Siluro-Devonian paragneiss and orthogneiss. (A) Geological contact; (B) syn- to post-Quaternary fault; (C) syn- to post-Plio-Quaternary fault; (D) syn- to post-Pliocene normal fault; (E) syn- to post-Miocene normal fault; (F) undated fault; (G) syn- to post-Quaternary thrust; (H) syn- to post-Pliocene thrust; (I) undated thrust; (J) undifferentiated fault; (K) boundary; (L) main river; (M) city. (c) Geological log of the Soultz EPS1 well [59, 115]. (d) Geological W-E cross section through Soultz-sous-Forêts based on a 3D geological modem from [116]. Common legend for (c) and (d).

Figure 2: Example of fracture in granite (a) with quartz filling (b) and alteration halo (c) (Ottenhöffen quarry, Germany).

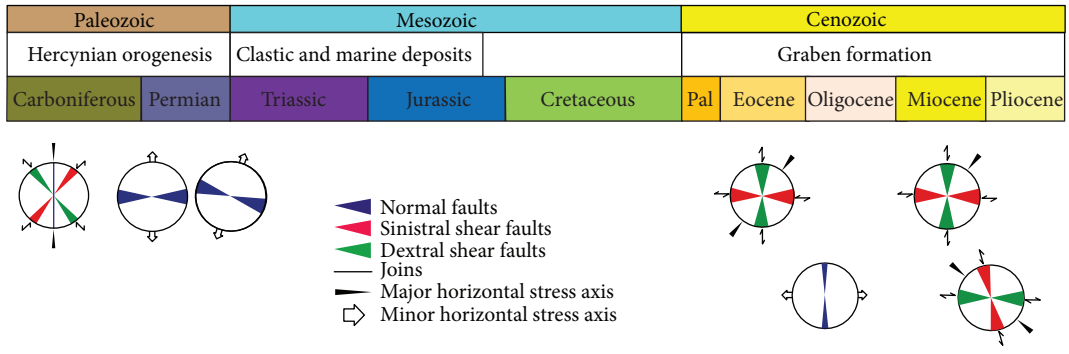

Figure 3: Synthesis of main brittle tectonic phases and associated fracture set directions since the Hercynian orogenesis in the Rhine graben and around the area modified after [117, 118] based on [37, 45, 48]. The circles represent the main orientation of fractures related to main stress axis (north on the top, east on the right).

graben as a result of the Africa-Europe collision [43, 44]. The first stage of this tectonic activity began during the Late Eocene with N-S compression, which affected the entire European continental platform (Figure 3) [45]. The primary phase of the opening of the Rhine graben took place during the Oligocene as a result of E-W extension (Figure 3). The direction of the stress axis did not vary, but the σ_1 and σ_2 axes reversed [45]. At this stage, normal faults appeared and blocks tilted (Figure 1(d)). The subsidence rate in the northern part of the graben differed from that of the southern part, which is bordered by the Erstein high. It constitutes the continuity between the Moldanubian and Saxo-Thuringian

zones [43, 46]. A second tectonic stage occurred during the Miocene with a succession of two compressions: NE-SW compression observed everywhere in the graben and characterized by upper mantle uplift [47] and NW-SE compression that continues today and causes left-lateral shear movement in the graben (Figure 3) [48].

In the southern part of the graben, the Vosges and Black Forest massifs were uplifted during the Mio-Pliocene, probably following the Alpine phase [49]. Today, the altitude difference of the Triassic and the Paleozoic basement boundary between the summit of the Vosges massif and the deeper part of the central graben is about 3000-4000 m (Figure 1(d)). This is evidence of substantial vertical movement.

The structure of the Rhine graben is slightly sinuous in form: the northern part trends N-S, the central part trends N30°E, and the southern part N10°E (Figure 1(b)). The graben boundaries are controlled by two types of major synthetic normal faults: the internal (Rhenane) and the external (Vosgian and Schwartzwaldian) faults. These faults outline the crescent-shaped fracture fields such as the Saverne fracture field (Figure 1(b)).

Over geological history, the graben has followed a thermal evolution related to the tectonic setting [6]. The pre-rift period corresponded to an uplift of the area without any associated thermal event, and the thermal gradient is considered as normal [38]. During the Eocene, a mantle diapir formed, in association with the first important thermal flux, inducing an abnormal thermal gradient up to 80°C/km in the upper crust [6]. During the Oligocene, volcanic activity occurred and substantial fault activation caused geothermal activity associated with fluid circulation [50]. After a phase of thermal attenuation, subsidence resumed during the Miocene and Pliocene epochs; it was more active in the north, associated with a third thermal phase which remains active today. Using the geothermal gradient proposed by Robert [6], the first maximum temperature of at least 100°C was reached at the beginning of rifting (Eocene) and may be associated with a mantle diapir. A second maximum temperature >100°C was reached during the late phase of the Rhine graben formation in the Miocene and remains active today. Present-day temperatures measured at the bottom of the sediment pile are about 130°C at a depth of 1400 m [51]. The highest gradients are measured on the western flank and are more developed in the northern part of the graben due to present-day tectonic activity [52].

2.2. EPS1 as a Reference Well inside the Rhine Graben. The deep EPS1 well, drilled in 1991 as part of the European EGS project at Soultz-sous-Forêts (Alsace, France) is a geological reference well in the Rhine graben because it is the only well cored to a depth of 2222 m (all depths are measured depth below ground level). This well was fully cored from 830 m to 2222 m, including 200 m in the lower Muschelkalk, 400 m in the Buntsandstein and Permian sandstones, and 800 m in the granite basement [53]. The Buntsandstein sandstones were reached at a depth of 1008 m under the Muschelkalk limestones, Permian sandstones at a depth of 1363 m, and the crystalline basement at a depth of 1417 m (Figure 1(c)). Because the European EGS project was designed to exploit deep geothermal energy, the granite basement was studied in more detail than the overlying Cenozoic and Mesozoic formations that the well encountered.

The Buntsandstein Vosgian sandstones in the EPS1 well are classified as moderately to well-sorted rounded lithic feldspathic arenites. They consist of dominant monocrystalline and polycrystalline quartz grains and K-feldspar grains with minor lithic grains and clays. Permian sandstones are for the most part heterogranular arkoses containing numerous lithic fragments, minor plagioclase, and more abundant clay minerals. More than 300 fractures were measured on the almost 400 m of the cored sandstones, and no slickenlines were observed. The fracture network shows limited scattering around N170°E, and dips are equally balanced between west and east (Figure 4). Within the well, some intervals are grayish and more intense fracture zones associated with a quartz-barite filling are present. A first deformation zone at 1012 m separates the Muschelkalk from the Buntsandstein formations. This fracture zone is probably a normal fault oriented N130°E-80°E [54]. Within the Buntsandstein sandstones, a large fracture zone is present between 1172 m and 1210 m corresponding to the boundary between the Upper and the Lower Vosgian sandstones (Figure 5). This fracture zone contains an isolated 2 cm-thick N20°E fracture at 1173.5 m, a network of mm-to-cm-thick N-S fractures reworking a cataclasis band between 1191 m and 1195 m, and a complex 5 m-thick N160°E fault zone at 1205-1210 m. The complete fracture zone is about 30 m thick in the well (Figure 5) [54]. It is assumed that this fracture zone intersects two other nearby wells, GPK1 and 4550, where total mud losses occurred when drilling through this zone [54].

The granite in the EPS1 well is a biotite-amphibole porphyritic monzogranite [55, 56] dated at $334.0 + 3.8/-3.5$ Ma (2σ) using zircon U-Pb age [57]. The granite is affected by a dense vein network and a high degree of alteration resulting from different generations of fracturation and fluid/rock interactions. Fracture fillings are heterogeneous, and polyphased, dominantly represented by major quartz, barite, pure white mica (illite), carbonates, and iron oxides [58].

More than 3000 fractures and several fracture zones have been identified in the granite between 1420 and 2222 m; they are fully described, and their orientation was measured in comparison to well images [59, 60] (Figure 6). Of them, 141 striated faults were observed and kinematic inversion showed four Cenozoic brittle tectonic phases with evidence of inherited faults [61]. These fractures are present as individual fractures and fracture zones, which are larger-scale (10-20 m) structures of highly clustered fractures [54, 58, 62]. They are grouped into two main sets roughly striking north-south (N005°E and N170°E with dips of 70°W and 70°E; Figure 6) [60]. Both sets are close to a conjugate fracture pattern of normal faults related to the Rhine graben formation [61]. Three secondary fracture sets were also identified, which are oriented E-W, NE-SW, and NW-SE (Figure 6). Moreover, the top of the granite is crosscut by numerous subhorizontal fractures that are characteristic of the top of the granite, attributed to a surface-stress relaxation effect that occurred when the batholith was unroofed during the

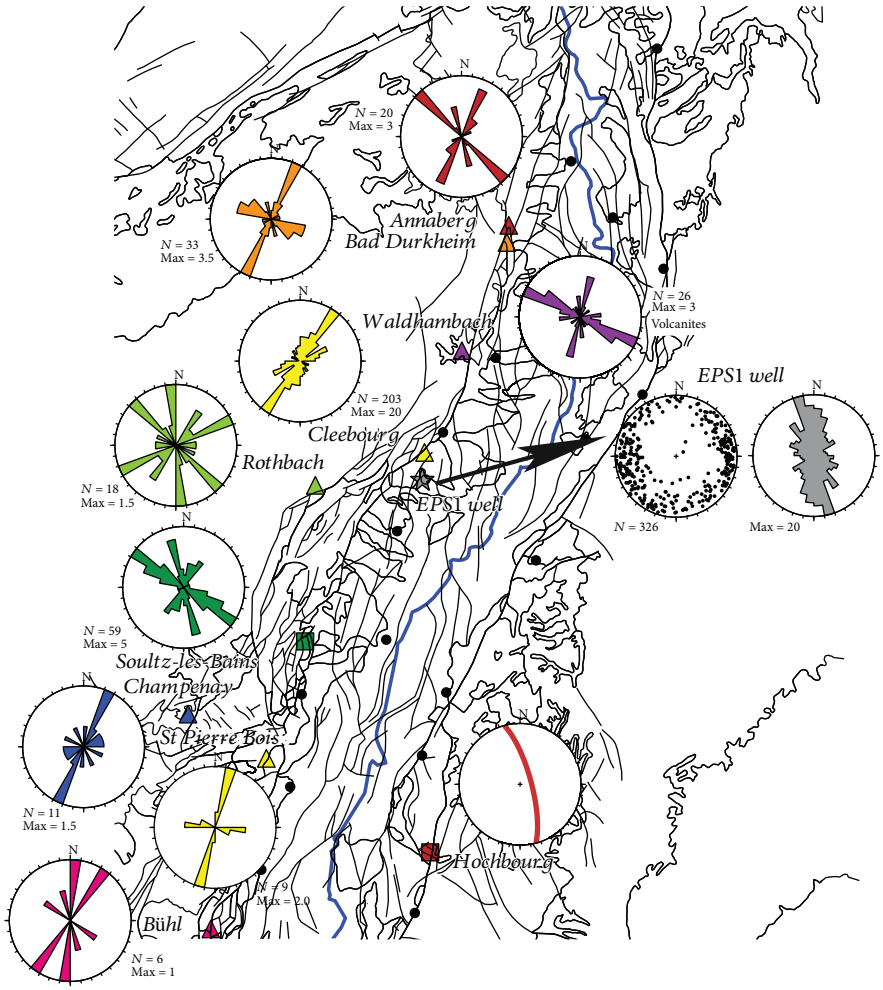

Figure 4: Fracture directions measured at the Permo-Triassic sandstone outcrops, including the measurements on cores of the EPS1 well and in Permian volcanic rocks at the Waldhambach quarry, represented on a structural map showing major structures. Bold lines represent the main faults and fine lines represent geological boundaries (same as Figure 1). For each site, the rose diagram shows the fracture directions in 10° classes. EPS1 well data, the plot diagram represents fracture pole in Schmidt's projection, lower hemisphere. The different colors correspond to each site. The location of the sites is indicated by a square for outcrops, a triangle for quarries, and a star for wells.

Permian (Figure 7) [60]. Because of the long geological history of the granitic basement, most fractures were reactivated during various tectonic phases depending on the relationship between the fracture orientation and the stress field direction [61]. Of the 3000 fractures, only five present an indication of previous fluid circulation [54].

Numerous studies have been conducted on hydrothermal alteration in the Soultz-sous-Forêts granite [60, 63–67]. This hydrothermal alteration is polyphase; early pervasive alteration affects the granite at a large scale, and later alteration is due to fluid circulation in the fracture network. Early pervasive alteration associated with rare fractures consists of a chlorite-epidote-carbonate retromorphic assemblage that affects granite even in the least fractured zones. Its role is negligible in reducing reservoir permeability [65, 68]. Fluids associated with this early alteration are moderately saline (2-7 wt% eq. NaCl) and were trapped under temperatures of 180-340°C on the basis of fluid inclusion microthermometry; they are considered to be of late Variscan age [69].

Hydrothermal alteration associated with fracture zones is dominant [70]. It results from interaction between granite and circulating fluids in the fracture network [71]. Hydrothermal minerals are quartz, clay minerals (illite, R3-type illite/smectite mixed layers, and tosudite), carbonates, barite, hematite, pyrite, and galena [54, 60, 68, 69, 72, 73]. Four primary highly fractured zones can be defined showing high content of hydrothermal minerals (Figure 7): (1) 1420-1530 m: quartz with hematite and carbonates, (2) 1620-1725 m: quartz with hematite and clay minerals, (3) 2050-2080 m: quartz with calcite and clay, and (4) 2155-2180 m: dominantly quartz [54]. Quartz-barite and quartz-ankerite veins containing a generation of lower-temperature brines (130°C–160°C) with a broad salinity range are attributed to younger, post-Oligocene up-to-the-present-day fluid-flow events [67, 69, 74]. The wall rocks of the fractures also frequently exhibit hydrothermal alteration and are marked by high porosity of up to 20% [68] due to alteration of primary minerals to clay minerals [73, 75, 76].

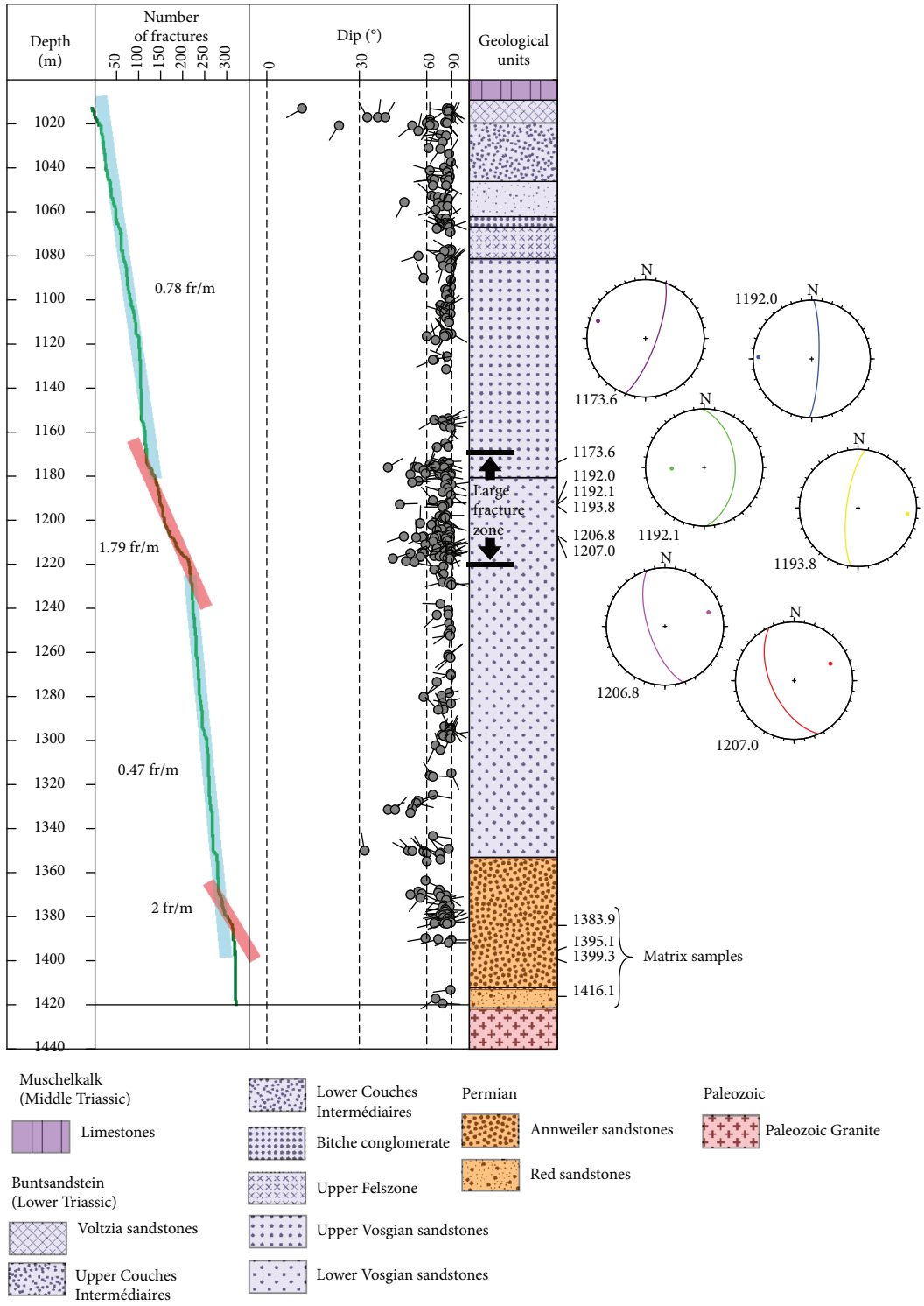

Figure 5: Composite log of Permo-Triassic sandstones in the EPS1 well. The first column represents the measured depth; the second, the cumulative fracture log; the third, the fracture orientation; the fourth, the geological units [115]. Sample locations are shown. The orientation (great circle and pole) of sampled fractures is represented in Schmidt's projection, lower hemisphere.

This fluid circulation within fracture and fault zones suggests that the contribution of convective heat transfer is dominant and explains the high temperature along the western margin of the graben [77, 78].

3. Rock Sample Collection

To discriminate between Hercynian and graben-opening brittle tectonics, we revisited the fractures in the EPS1 well,

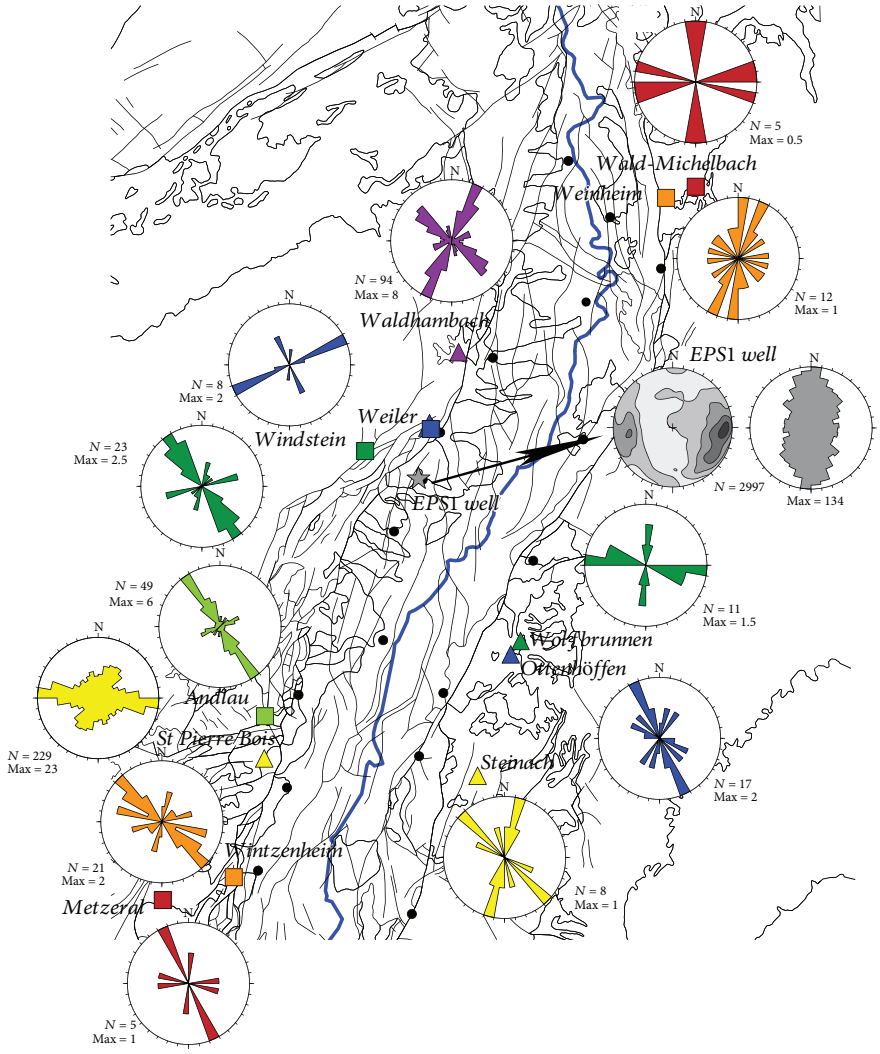

FIGURE 6: Fracture directions measured on Paleozoic basement outcrops including the measurements on EPS1 well cores, represented on a structural map showing major structures. Bold lines represent the main faults, and fine lines represent geological boundaries (same as Figure 1). For each site, the rose diagram shows the fracture direction with 10° classes. For EPS1 well data, contour-density diagrams in Schmidt's projection, lower hemisphere: 10%, 30%, 50%, 70%, and 90% of the fracture pole maximum frequency. The different colors correspond to each site. The location of the sites is indicated by a square for outcrops, a triangle for quarries, and a star for wells.

which is located within the Rhine graben, and compared them to fracture analysis on surface Hercynian and Permo-Triassic outcrops at 20 different sites in the Vosges and the Black Forest massifs (Figure 1(b)).

Except for the Hochburg outcrop, the eight Permo-Triassic sites are along the western border, in the Vosges massif, and in the Saint Pierre Bois and Waldhambach quarries, where both Permo-Triassic formations and Hercynian basement are present (Figure 1(b), Table 1). The 12 sites in the Hercynian basement are distributed equally on the western and eastern borders of the Rhine graben (Figure 1(b)).

Generally, these sites are quarries, either abandoned or producing, but some sites are outcrops along roads (Hochburg, Windstein, and Andlau). The quarries in the Hercynian basement exploit granite and gneiss-type rocks for rock fill, and quarries in Permian and Buntsandstein sandstones extract building stones. Except for Weiler and Andlau, which are metamorphic rocks, the other basement sites are granite (Table 1).

On the outcrops, we first measured fracture orientations to determine the statistical fault pattern and the primary sets for each site. Some sites have several outcrop directions allowing good fracture sampling (Table 1). Second, we sampled fracture infills in relation to the orientation of the fractures themselves and if possible, we oriented the samples in relation to north and to the horizontal plane.

In our study of the EPS1 Soultz well, we examined more than seventy thin sections of available cores of Triassic sandstones and Hercynian granite. Based on previous work and on these observations, we selected seventeen representative samples:

(1) six samples from the most fractured interval in the Buntsandstein sandstones, between 1170 and 1210 m, in a large shear zone (Figure 5)

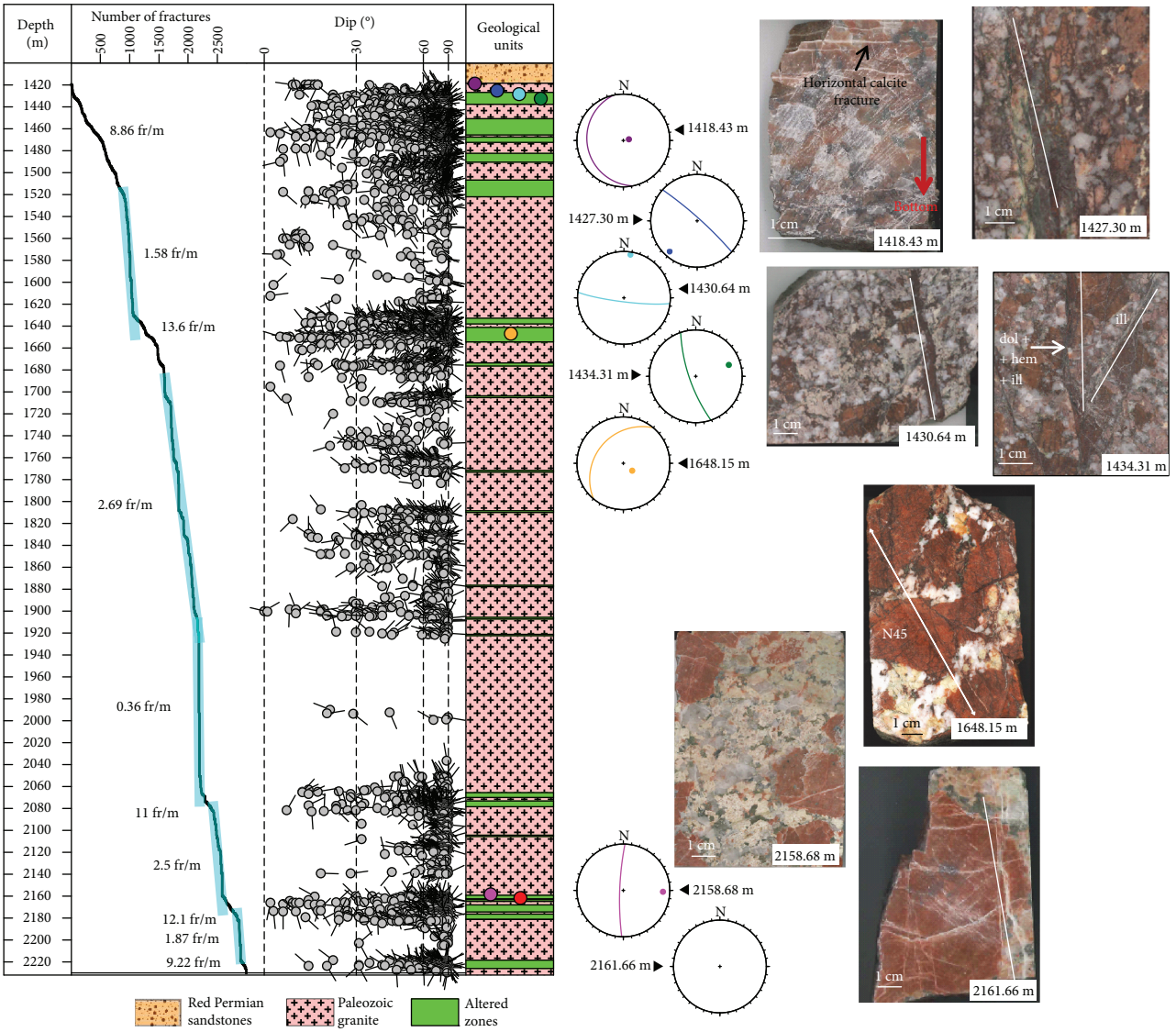

FIGURE 7: Composite log of Hercynian granite in the EPS1 well. The first column represents the measured depth; the second, the cumulative fracture log; the third, the fracture orientation; the fourth, the geological units [60]. The location and macroscopic pictures of samples are shown. The orientation (great circle and pole) of sampled fractures is represented in Schmidt's projection, lower hemisphere.

(2) four samples of the Buntsandstein/Permian sandstones near the sedimentary cover/granite interface between 1382 and 1416 m (Figure 5)

(3) four samples at the top of the pluton and specifically in the 20 meters below the sedimentary cover/granite interface, between 1417 and 1435 m (Figure 7)

(4) one sample at about 1650 m in a fracture zone (Figure 7)

(5) two samples close to the deepest fractured zone at 2158 m and 2161 m (Figure 7)

Of the six samples collected in the most fractured interval of the Buntsandstein sandstones, one sample at a depth of 1173.6 m contains an isolated fracture, three samples at depths of 1192.0 m, 1192.1 m, and 1193.8 m belong to a zone characterized by a high fracture density, and two samples at 1206.8 and 1207 m belong to the major fault zone.

In the granite, the seven large mineralized fractures have various orientations and mineral filling is studied in relation to fracture orientation (Figure 7). The upper sample is located at a depth of 1418.43 m, on the top of the granite, within the paleoweathering alteration zone (Figure 7). The fracture is oriented N170°E-14°W. This zone is characterized by a high density of subhorizontal fractures (about 9 fr/m) with a N-S average direction, attributed to a surface-stress relaxation effect during unroofing of the batholith in the Permian [60].

The three fractures at the top of the granite are located at depths of 1427.30 m, 1430.64 m, and 1434.31 m in the same

Table 1: Description of sampling sites, outcrops, and quarries, with age and type of rock, type of site, and main direction of fracture measurement scanlines.

Site name	Age	Type of rock	Description of the site	Longitude	Latitude
Annaberg	Buntsandstein	Light-colored and leached sandstones	Two small exploited quarries. Main direction of walls: NE-SW.	8.15503	49.4793
Bad Dürkheim	Buntsandstein	Beige leached sandstones	Old abandoned quarry, exploited by the Romans. Large and high wall oriented NE-SW and NW-SE.	8.15768	49.4643
Cleebourg	Buntsandstein	Pink and yellowish leached sandstones.	Small exploited quarry for ornamental stones. Large fault, enclosed in the Western Rhenane fault, intersects the quarry. Main direction of the walls: N20°E and N110°E.	7.891	49.013
Rothbach Loegel	Buntsandstein	Pink sandstones	Large quarry exploiting ornamental stones within caves. In the caves, fractures can be observed on N120°E and N30°E direction, on the roof and the footwall.	7.51753	48.9131
Soultz-les-Bains	Top of Buntsandstein (Volzia) with the transition of the shelly sandstones of Muschelkalk	Beige sandstones	Abandoned quarry, namely, "Carrière Royale". Very tall wall with NW-SE direction and several meters long.	7.49556	48.5715
Bühl	Buntsandstein	Pink sandstones	Abandoned small quarry exploited until the 30s. Very tall wall with NW-SE direction.	7.18677	47.9344
Hochburg (Sexau)	Buntsandstein	Pink sandstones	Outcrop under the medieval castle.	7.89997	48.1167
Champenay	Permian	Coarse-grained pink sandstones	Exploited quarry for ornamental stones. Main direction wall: NW-SE and NE-SW.	7.1115	48.412
Waldhambach	Paleozoic/Triassic	Pink Buntsandstein sandstones, Permian arkose (Rotliegende) and volcanites (melaphyr), Hercynian granodiorite	Large granite quarry exploited for rock fill. The main accessible part is in granodiorite. The granodiorite is highly fractured. NW-SE lamprophyre dikes crosscut the granodiorite.	8.00256	49.1609
Saint Pierre Bois	Paleozoic/Triassic	Permian sandstones and Hercynian granite.	Exploited quarry in the granite for rock fill. Main direction of the walls: NW-SE and NE-SW.	7.3678	48.3323
Weiler	Paleozoic (Devonian)	Schistes, grauwackes, and volcanites (metamorphic volcano-sedimentary pile (Ménillet et al., 1989))	Small old quarry. Main wall oriented N-S.	7.90106	49.0436
Windstein	Paleozoic (Visean)	Altered coarse-grained biotite-amphibole-granite	Outcrops.	7.68175	48.9844
Andlau	Paleozoic (Visean)	Schists and hornfels	Several scattered outcrops.	7.36813	48.3942
Wintzenheim	Paleozoic (Visean)	Altered biotite-rich porphyritic granite	Outcrops scattered along the Western Rhenane fault.	7.27503	48.073
Metzeral	Paleozoic (Visean)	Altered coarse-grained biotite-amphibole- granite	Small outcrops in front of the quarry of coarse grain granite	7.08378	48.0213
Steinach	Paleozoic	Fine-grained granite	Large exploited quarry of granite and outcrops along the road. Main wall direction: NW-SE and NE-SW. Large fault filled by cm-sized euhedral calcite crosscut the granite.	8.06116	48.2943

Table 1: Continued.

Site name	Age	Type of rock	Description of the site	Longitude	Latitude
Ottenhöffen	Paleozoic	Highly altered granite	Small quarry exploited for sand. Main wall oriented E-W. Pieces of rocks, not in place, show vuggy quartz, cockade breccia, siliceous breccia, and finely siliceous banded veins suggesting intense low-temperature hydrothermal circulation	8.16231	48.5568
Wolfsbrünnen	Paleozoic	Slightly altered fine-grained granite	Large exploited quarry	8.62357	49.0143
Weinheim	Paleozoic		Outcrops in front of the exploited quarry. Contact between the two granites is a large mineralized fault exploited for silver during the 15th century (personal communication).	8.68631	49.5549
Wald-Michelbach	Paleozoic	Pink feldspar-rich granite-like syenite	Abandoned quarry. NW-SE main outcrops.	8.79013	49.5811

upper fractured zone (Figure 7). The fractures have various orientations: N130°E-80°NE; N100°E-80°S, and N160°E-75°SW, respectively (Figure 7). The fracture at a depth of 1648.15 m, oriented N40°E-30°NW, is contained within an open fracture zone showing geodic quartz and that has a thickness along the well of about 20-30 cm (Figure 7) [79]. The two deeper fractures are located in the 2100 m fracture zone, at depths of 2158.68 m and 2161.66 m, respectively (Figure 7). The first fracture is oriented N-S, exactly at N0°E-80°W, whereas the second is oriented NW-SE, N150°E-85°NE (Figure 7). During drilling operations, both partial mud losses and natural outflow were observed at this depth [54]. The cores show thick quartz vein deposition in these two locations, characterized by very low gamma ray values. In the peripheral area of the quartz vein, the hydrothermally altered and cataclastic granite corresponds to increased gamma ray values [58]. This increase is characteristic of clay deposition. This zone ranges in thickness from 20 to 30 m in the well.

In the eastern part of the graben, the Heidelberg well (He01; Figure 1(b)) was fully cored from the surface through the Buntsandstein sandstones to 146.70 m below ground level and through the Heidelberg granite down to a depth of 153 m. The Heidelberg granite is a beige-pink porphyritic biotite monzogranite [80]. However, because these cores were not oriented, fracture orientations could not be determined, but the fracture infills were analyzed to complete the observations.

4. Analytical Techniques

4.1. Mineralogical Characterization

4.1.1. Microscope Observations. Optical observations were carried out using an Olympus BH2 microscope under transmitted and reflected light. Complementary observations and analyses of polished thin sections of samples were performed on a scanning electron microscope (SEM) coupled with an energy-dispersive spectrometer (Kevex Quantum) tuned at 25 kV. Prior to analysis, a 10–20 nm-thick carbon layer was sputter-coated on polished thin sections (Edwards Auto 306).

Cathodoluminescence was used to discriminate carbonates precipitated from different fluids because it is a sensitive method for tracing element contents and their crystalline framework. Mn^{2+} ion and trivalent REE ions appear to be the most important activator ions of extrinsic CL, whereas Fe^{2+} is the main quencher [81, 82]. The system used was a cold cathode Cathodyne manufactured by the OPEA Society (Laboratoire Optique Electronique Appliquée). The electron beam has adjustable energies up to 26 keV and currents up to 250 μA. The cathodyne is mounted on an Olympus microscope allowing magnification up to 200. The system is equipped with a JVC KYF75U tri-CCD digital camera. The three 12 mm-sized sensors have a resolution of 1360 × 1024 pixels. Calcite was distinguished by its yellowish orange color; dolomite by its dark red orange to light red orange color, and ankerite by its dark color due to inhibition of extrinsic luminescence by iron.

4.1.2. Electron Microprobe. Spot analyses of carbonates and sulfates were performed on polished thin sections of samples covered with a carbon coating, using a CAMEBAX SX50 electron microprobe with an acceleration voltage of 15 kV, a current beam of 12 nA, and a 1–2 lm beam width. Peak and background counting times were 10 s for major elements. Standards used included both well-characterized natural minerals and synthetic oxides. Matrix corrections were made with a ZAF computing program.

4.2. Isotopic Analysis Techniques

4.2.1. Carbon and Oxygen Isotopes of Carbonates. The conventional method by Rosenbaum and Sheppard [83] was used to extract calcite and dolomite, successively. We analyzed the resulting CO_2 samples for their isotopic compositions using a Delta S Finnigan MAT gas-source mass spectrometer.

4.2.2. Oxygen Isotopes of Quartz. In situ oxygen isotopic compositions of quartz were measured on polished thin sections using SIMS with a Cameca IMS 1280 ion microprobe at CRPG in Nancy (France). Prior to analysis, a 10–20 nm-thick gold layer was sputter-coated on polished thin sections. Analyses were performed using a Cs primary ion beam of 10 keV, a current of 0.5 nA, and a beam size of 15 μm. Secondary ions were accelerated by applying a nominal voltage of -4.5 kV, the energy window was set to 35 eV, and no offset was applied. Quartz references were analyzed each day at the beginning and at the end of the day, to calculate the instrumental mass fractionation (IMF), as follows:

$$\mathrm{IMF} = \delta^{18}\mathrm{O}_{\mathrm{std\,ref}} - \mathrm{average}\left(\delta^{18}\mathrm{O}_{\mathrm{std\,meas}}\right)_n, \quad (1)$$

where $\delta^{18}\mathrm{O}_{\mathrm{std\,meas}}$ is the oxygen isotopic composition of the reference by ion microprobe, $\delta^{18}\mathrm{O}_{\mathrm{std\,ref}}$ is the oxygen isotopic composition of the standard, and n is the number of analyses. The quartz $\delta^{18}\mathrm{O}$ measured by the ion microprobe ($\delta^{18}\mathrm{O}_{\mathrm{Quartz\,meas}}$) was corrected from the instrumental fractionation (IMF) as follows:

$$\delta^{18}\mathrm{O}_{\mathrm{Quartz\,corr}} = \delta^{18}\mathrm{O}_{\mathrm{Quartz\,meas}} + \mathrm{IMF}_{(\mathrm{quartz})}. \quad (2)$$

All results are reported in δ units relative to international standards, defined by $d = (R_{\mathrm{Sample}}/R_{\mathrm{Standard}} - 1) \times 1000‰$, where R is the measured isotopic ratio in the sample and in the standard: standard mean ocean water (SMOW) for oxygen and Pee Dee Belemnite (PDB) for carbon. Reproducibility was ±0.2‰ for oxygen and carbon.

4.2.3. Strontium Isotopes in Dolomite and Barite. Strontium isotopic ratios were measured in dolomite and barite separated by hand picking on thin sections. Strontium was extracted by adding 10 mL of 6 N HCl solution (extra-pure-quality concentrated HCl) to crushed mineral separates in covered Teflon beakers.

The leachate was purified using an ion-exchange resin (Sr-Spec) before mass analysis according to a method

adapted from Pin and Bassin [84], with blank <1 ng for the entire chemical procedure. After chemical separation, ~150 ng of Sr was loaded onto a tungsten filament with tantalum activator and analyzed using a Finnigan MAT 262 multicollector solid source mass spectrometer (Bremen, Germany). The $^{87}Sr/^{86}Sr$ ratios were normalized to a $^{86}Sr/^{88}Sr$ ratio of 0.1194. An average internal precision of 10 ppm (2 sm) was obtained, and the reproducibility of the $^{87}Sr/^{86}Sr$ ratio measurements was tested through repeated analyses of the certified NBS987 standard (0.710240).

5. Results

5.1. Permo-Triassic Formations

5.1.1. Matrix Diagenesis. Sandstones sampled in quarries on both flanks of the Rhine graben are similar to sandstones located within the Rhine graben reached by well EPS1. Buntsandstein sandstones are generally reddish, but others are white to gray, including those from the Cleebourg, Soultz-les-Bains, Bühl, and Bad Durkheim quarries and from the Hochburg outcrop, due to the absence of hematite. Some of these quarries are located inside the Western Rhenane boundary fault (Bühl, Cleebourg; Figure 1(b)) or have high fracture density (Bad Dürkheim, Soultz-les-Bains) where fluids have circulated intensely and remobilized iron from iron oxides and hydroxides.

The Buntsandstein and Permian sandstones consist essentially of monocrystalline and polycrystalline quartz grains, feldspar grains, lithic grains, and clays. K-feldspar is the major feldspar observed in these sandstones (Figure 8). The K-feldspar content of Buntsandstein sandstones in the EPS 1 well is estimated to be about 15%. Plagioclase is almost absent in Buntsandstein sandstones, whereas it is present in Permian sandstones.

Diagenesis in the Buntsandstein and Permian sandstones is marked by various degrees of alteration and dissolution of detrital minerals and by formation of authigenic minerals including dominant quartz, illite-like clays with minor alkali feldspar, barite, carbonates, and hematite (Figure 8), except in a few samples of Permian sandstones from the Waldhambach quarry where authigenic minerals are mostly absent. When authigenic minerals are present, they everywhere exhibit the same features as the samples from the EPS1 well and from the various outcrops (excluding Waldhambach).

Stability of detrital minerals is of primary importance in porosity evolution. Feldspar minerals including K-feldspar and plagioclase in Permian sandstones exhibit various degrees of alteration to microphyllites, which modifies the porosity. Detrital K-feldspar also exhibits various degrees of dissolution that give rise to secondary porosity in the Buntsandstein and Permian sandstones located both inside and outside the Rhine graben.

Authigenic illite-like clays (Ilt) are observed in small amounts in all sandstones (Figure 8). Clays essentially occur as early radial fibers growing on detrital quartz (Qz0) and K-feldspar grains (Kfs0) (Figures 8(c)–8(e)). Their presence generally inhibits the growth of quartz aureole.

Rare authigenic K-feldspar (Kfs1) is observed in all sandstones (Figure 8(h)). Authigenic K-feldspar grows as small euhedral crystals on detrital K-feldspar grains. Electron microprobe analyses show that unlike detrital K-feldspar (Kfs0), the authigenic K-feldspar (Kfs1) do not contain Ba. Authigenic and detrital K-feldspar both exhibit signs of dissolution, indicating that authigenic K-feldspar formed prior to the dissolution process.

Authigenic quartz occurs predominantly as overgrowths on detrital quartz (Qz1) (Figures 8(b), 8(e), and 8(h)) but also as microcrystalline grains associated with illite-like clays (μQz + Ilt) (Figures 8(b)–8(d), 8(g), and 8(h)) and as late fillings in dissolution cavities in K-feldspar (Qz2).

Barite (Brt) and carbonate cements grow on authigenic radial illite-like clays, quartz overgrowths, K-feldspar overgrowths, and illite-like clays, and microquartz assemblages; they also fill dissolution cavities in K-feldspar. These observations indicate that they precipitated later than all previous authigenic phases and also later than the K-feldspar dissolution process (Figures 8(g) and 8(h)). Whereas traces of barite are present everywhere in the EPS1 well sandstones, carbonates are abundantly present in the sandstones between 1382 and 1416 m near the interface with the Hercynian basement. The carbonates occur as large euhedral or poekilitic crystals that exhibit a relatively homogeneous red-orange color under cathodoluminescence (CL), with minor dark red zoning.

5.1.2. Fracture Description in Well EPS1 inside the Graben. In the well EPS1, the average fracture density in Buntsandstein and Permian sandstones is less than 1 fracture/m. Two other zones are more highly fractured; one of them is present between 1170 and 1220 m in the Vosgian sandstones, and the other is between 1370 and 1382 m in the Annweiler sandstones, with 1.79 and 2 fractures/m, respectively (Figure 5). The fracture network shows limited scattering between N20°E and N170°E, and dips are equally balanced between east and west (Figure 4).

Between the depths of 1170 and 1210 m within a large fracture zone (Figure 5), we distinguish two fracture types based on texture and fill descriptions. In the first type of fracture, which strikes N-S and dips to the west, cataclastic textures that are highly cemented with microcrystalline quartz and illite-like clays (μQz + Ilt) are observed at 1193.8 m, 1206.8 m, and 1207 m (Figure 5). Grains of partially dissolved K-feldspar are observed in the cataclasis. Considering the fragility of the partially dissolved K-feldspar, their presence strongly suggests that the dissolution process took place after the cataclasis. In wall rock of the fractures, an illite-like clay and microcrystalline quartz association was also observed at grain boundaries and in crosscutting elements.

The second fracture type, which can be observed at 1173.6 m, 1192.0 m, 1192.1 m, and 1206.8 m, is also not far from N-S but dips to the east (Figure 5) and at a depth of 1207 m exhibits mm- to cm-thick fractures filled by euhedral quartz or barite. In the fault zone at 1206.8 and 1207 m, veins of euhedral quartz and barite crosscut cohesive cataclasite, suggesting that these fillings are later than cataclasis and associated cementation. Fractures at 1173.6 m contain both

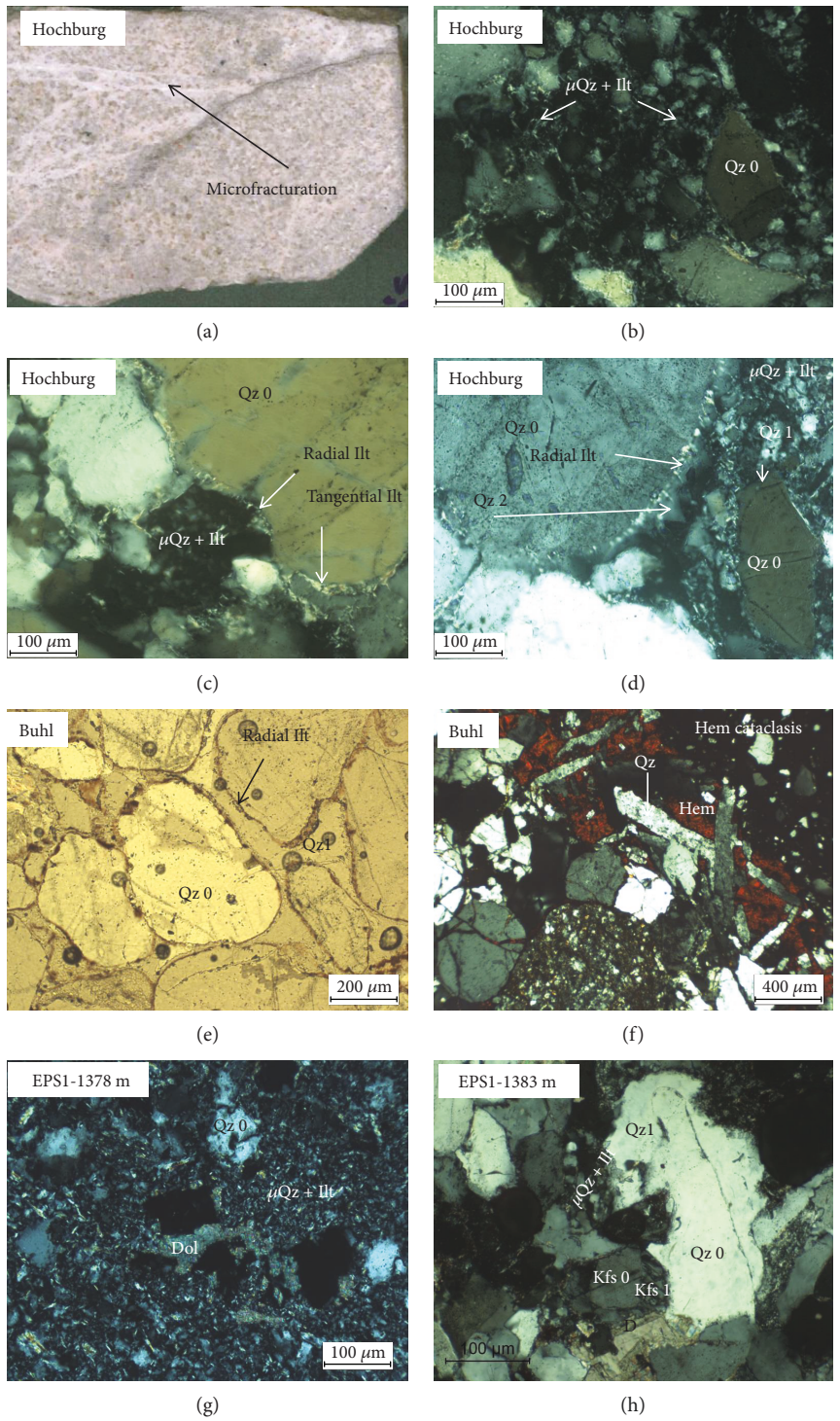

Figure 8: Fractures and matrix along fractures in sandstones. (a, b, c, d) Example from Hochburg: (a) Whitish and microfracture cutting across sandstone; (b) microscopic image of whitish microfractures that provide evidence of cohesive microcataclasite cemented by microquartz (μQz) and illite (Ilt) (polarized light); (c) detail of the matrix along the whitish microfracture, showing microquartz and illite (μQz + Ilt) and cements of radial illite and tangential illite (polarized light); (d) another detail of the matrix showing quartz overgrowth, cement of microquartz and illite, and growth of radial illite on detrital quartz cemented by diagenetic quartz (Qz1) (polarized light); (e, f) example from Buhl: (e) matrix of fractured sandstone showing massive quartz cementation (Qza) of detrital quartz surrounded by radial illite (natural light); (f) cohesive microcataclasite cemented by quartz and hematite (Hem), then crosscut by a vein of quartz and hematite (polarized light); (g, h) Examples from EPS1 well: (g) fracture at 1378 m showing cohesive cataclasite cemented by microquartz and illite, then crosscut by dolomite filling (polarized light); (h) sandstone matrix at 1383 m showing late dolomite cementing all the earlier authigenic minerals (polarized light).

quartz and barite. In this last case, barite occurs in the center of the fracture indicating that barite precipitated later than quartz. In the sandstone matrix near the quartz-filled fractures, quartz cement noted/identified as Qz2 (porosity plugging by quartz, euhedral quartz) is well developed in intergrain porosity and in K-feldspar dissolution porosity, suggesting that the K-feldspar dissolution process occurred prior to quartz filling; barite cement is rare at contacts with barite fractures. Carbonates are not present in fractures that crosscut the sandstone, but their relationships with other diagenetic minerals strongly suggest that carbonates precipitated later than the first generation of fractures associated with cataclasis and the K-feldspar dissolution process.

5.1.3. Fracture Description of Outcrops outside the Graben. Whereas numerous fractures were measured in the field, no slickenlines were observed. The Annaberg and Bad Dükheim quarries exhibit large fracture planes, almost regularly spaced out with a fracture density of approximately 1-2 fractures/m. At Cleebourg, the density is similar, approximately 1.3 fracture/m, but the density is not everywhere homogeneous and it increases closer to the Rhenane border fault, which cuts across the quarry (Figure 1(b); [85]). Although the Rothbach quarry is located close to the Vosgian fault at the border/margin of the Saverne fracture field (Figure 1(b)), fracture density is low, less than 0.5 fracture/m, making it possible to explore for ornamental rocks. Like Cleebourg, the Soultz-les-Bains quarry is highly fractured due to the presence of a large fault. Fracture density is approximately 3 fractures/m. At Bühl, in the Vosgian sandstones, large fracture planes cut across the Vosgian sandstones with a density of approximately 1 fracture/m.

In the Permian sandstones of the Saint Pierre Bois and Champenay quarries, fracture density is similar, approximately 1-2 fractures/m, even though they do not have the same spatial relationship to the Rhenane fault; Saint Pierre Bois is near the fault and Champenay is more distant (Figure 1(b)).

The fracture orientations depict an approximately N-S fracture set present in all outcrops of the Buntsandstein, corresponding to the average direction of the graben border fault (Figure 4). However, this is not always the major set, as at Annaberg and Soultz-les-Bains, where a NW-SE fracture set is dominant. The N170°E direction, very common in the EPS1 well, is less common at the surface, except at Rothbach and Soultz-les-Bains (Figure 4).

In the Waldhambach quarry, a large Permian volcanic lava flow overlies the Permian sandstone and underlies the Buntsandstein sandstones. These Permian volcanic rocks are highly hydrothermally altered and fractured. The two major fracture sets are N110°E-N130°E and N10°E-N20°E (Figure 4). Both sets are consistent with those in the Permo-Triassic sandstones, whereas the N110°E set is not present in the Permian sandstones of Champenay (Figure 4).

Sandstone cementation is minor and is characterized by growths of quartz aureoles (Qz1), K-feldspar, and radial illite-like clays. Fractures observed in sandstones collected in quarries seem poorly filled in the field: microscopic observations confirm few fillings in fractures and rare cataclastic textures. At Champenay, quartz cementation (Qz2) is observed in sandstone near a N15°E fracture. Faults and fractures striking N160°E to N170°E at Hochburg and Bühl are associated with cataclasis textures and cemented by microcrystalline quartz and illite-like clays (μQz + Ilt) (Figures 8(a) and 8(b)). This filling is also present in matrix cement near cataclastic planes. At Bühl, several N20°E quartz-hematite (Hem) veins associated with quartz cementation of the close matrix have been reworked in cataclastic planes (Figures 8(e) and 8(f)).

5.2. Paleozoic Basement

5.2.1. Fracture Description in Well EPS1 inside Graben. In the first (1418.43 m, 1427.30 m, 1430.64 m, and 1434.31 m) and second (1648.15 m) fracture zones (Figure 7), alteration of the granite matrix consists of (a) extensive sericitization of plagioclase, (b) illite-like clays + titanium oxides that replace early ferromagnesian minerals (biotite, amphibole, and muscovite), and (c) quartz + carbonate + titanium oxides that replace titanite.

At 1418.43 m, the sample contains numerous subhorizontal fractures (Figure 7) that are characteristic of the top of the granite; they are attributed to a surface-stress relaxation effect that prevailed during unroofing of the batholith in the Permian period [60]. Fracture fill consists of carbonates that have a homogeneous red-orange color under CL. Where numerous carbonate veins crosscut ancient biotite, the biotite is entirely replaced by illite-like clays + carbonate (red-orange under CL) + hematite. Where micron-sized fissures penetrate into biotite sheets, the biotite is replaced by yellowish illite with fibrous carbonate (dark red under CL) intercalated in the sheets.

The sample at 1427.30 m contains a NW-SE-oriented and centimeter-thick reddish fracture zone whose infilling is clearly polyphase (Figure 9). The first stage consists of a cohesive cataclasite cemented by illite-like clays and microquartz and rimmed by massive oriented sericite; some micron-sized monazite grains are associated with this early stage. The second stage consists of euhedral quartz and the third stage of gray carbonate (red-orange under CL) alternating with minor light-colored carbonate (dark red under CL). Minor barite (Brt) is observed in residual porosity in dolomite. The wall rock consists of altered granite marked by sericitization and iron oxide and carbonate precipitation in the secondary porosity of dissolved plagioclase. Carbonates in the wall rock have the same red-orange color under CL as dominant carbonates filling the fracture (Figure 9).

At 1430.64 m, the sample contains an E-W-oriented and 5 mm-thick dark reddish fracture within subeuhedral dark carbonate with minor euhedral quartz that crosscuts the granite (Figure 7). The color of the carbonate is largely due to an abundance of μm-sized iron oxide particles. Carbonates are red under CL. Under the microscope, the carbonate filling and the granite matrix are crosscut by an independent network of μm fissures of illite-like clays ± quartz. This texture strongly suggests that the illite/muscovite fissure network is later than the carbonate fissure network.

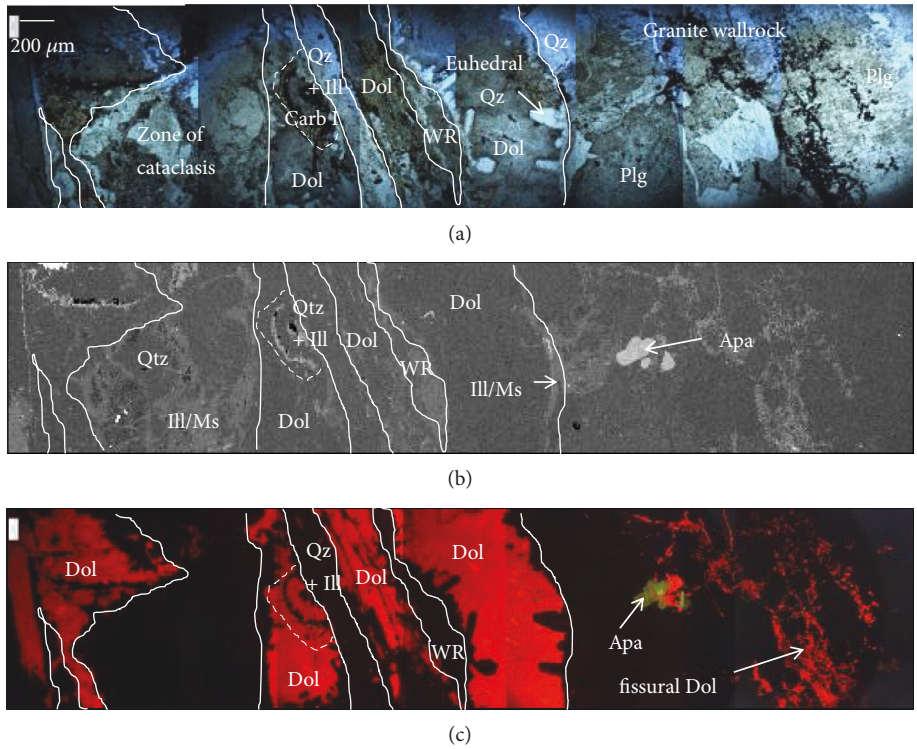

Figure 9: Image in transmitted natural light (a), backscattered electron image (b), and CL image (c) of a NW-SE mm-thick fracture and its granite wall-rock (WR) (EPS1-1427.30 m core sample) (images modified from [119]). Combined images provide evidence of polyphase filling of the fracture including a first stage of cataclasis cemented by quartz (Qz) and illite-muscovite (Ill/Ms) followed by euhedral quartz, then carbonate (dolomite) well identified by its red-orange color under CL. On the right side of the images, alteration of the wall-rock is marked by partial dissolution of plagioclase (Plg), precipitation of carbonate in secondary porosity in dissolved plagioclase and alteration of primary apatite (Apa) well identified by CL by yellowish-green color.

The sample at 1434.31 m contains two subparallel NNW-SSE <5 mm reddish fractures, the largest one being crosscut by a fine white illite-like clay fissure plane (Figure 7). The mineral infilling sequence is almost the same as that of sample at 1427.30 m. However, the microtextures are slightly different, because here the microfissures have only one filling (sericite + microquartz or carbonates that have red and dark red colors under CL). Moreover, the residual porosity is filled by carbonates (dark red under CL) and limpid quartz. Although illite fissures macroscopically seem to crosscut the reddish carbonate fracture, microscopically carbonate infills residual porosity and crosscuts an illite-like clay + quartz cataclastic zone.

At 1648.15 m, the sample is crosscut by a network of microfissures related to a NE-SW ~5 mm thick fracture (Figure 7). The fracture corresponds to a network of subparallel illite ± quartz fissures. Carbonate (dark red under CL) occurs as a discontinuous filling in this network and penetrating the granite matrix and forming a 200-300 μm-thick vein.

In the third fracture interval, the EPS1 granite has reddish silicified zones alternating with pink less-altered zones. The fracture density remains high (Figure 7). The mineralogy of the highly altered granite matrix at 2158.68 m is similar to that observed in both the first and second fracture intervals. In a less altered sample at 2161.66 m, remnant chlorite and titanite phantoms occur in the place of primary biotite. This assemblage is the early metamorphic/hydrothermal identified in the EPS1 granite. At 2158.68 m, the sample is crosscut by a network of carbonate (yellow-orange color under CL) fissures (Figure 7). A few fibrous carbonate lenses (dark red under CL) are observed in sheets of altered biotite. At 2161.43 m, the sample is crosscut by a NW-SE fracture and by a network of fissures filled predominantly by carbonate (dark red color under CL) with minor quartz (Figure 7). As we observed in the sample at 1418.43 m, dark carbonate under CL occurs as fibrous lenses intercalated in sheets of altered biotite. Yellow red carbonate under CL is present in altered plagioclase and also in a several fine veinlets crosscutting granite and also in sheets of altered biotite.

5.2.2. Fracture Description of Outcrops outside the Graben. Most granites that crop out in this study area are highly fractured, but the few striated faults that were observed were not enough to perform a significant kinematic inversion for this study. The fracture density ranges between one to more than ten fractures/m, as in the EPS1 well (Figure 7). Most sites, mainly in the Vosges and the northern Black Forest, as well as Wald-Michelbach, Weinheim, Waldhambach, Windstein, Weiler, Saint Pierre Bois, Metzeral and Wintzenheim, have rather homogeneous fracturing, with a fracture density of less than 5 fractures/m. Outcrops in the Southern Black Forest, Wolfbrunnen, Ottenhöffen, and Steinach quarries have a fracture density of more than 5 fractures/m with large

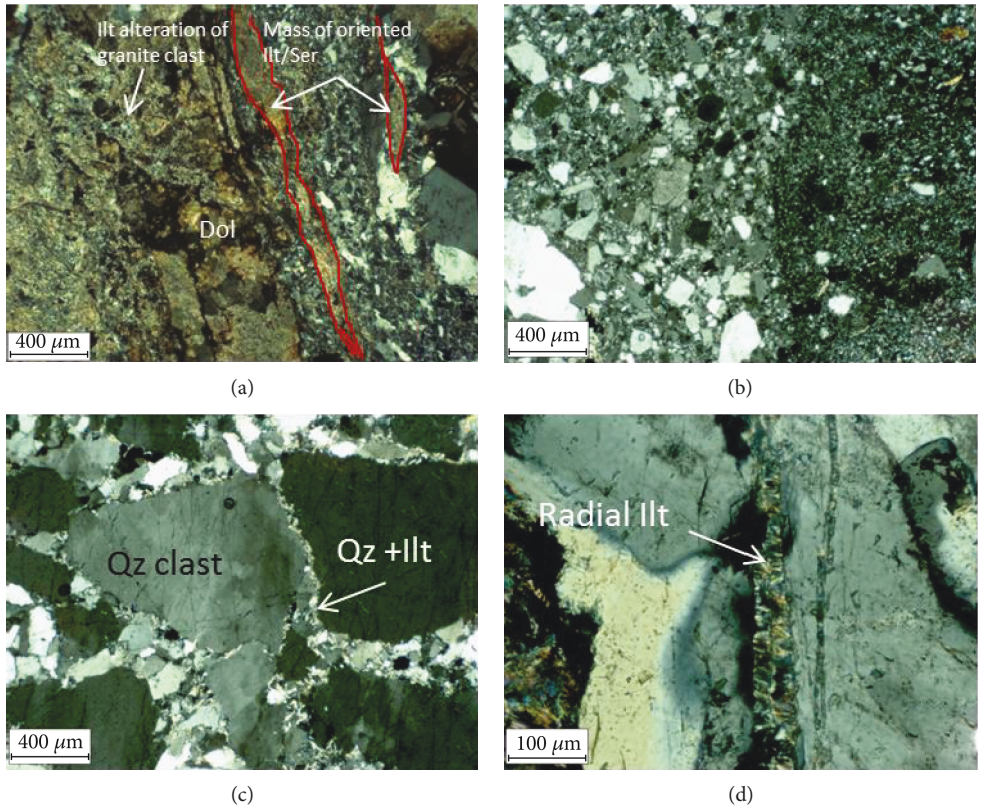

Figure 10: Microphotographs in polarized light of different types of fractures affecting granites on the flank of the Rhine Graben (images modified from [119]): (a) shear/cataclasis with sericite mass/granite clasts in a NW-SE fracture (Waldhambach); (b) cataclastic texture in a E-W fracture (Saint Pierre Bois); (c) protocataclasis of a N50°E quartz vein crosscutting Wintzenheim granite; (d) N170°E fissure filled with radial illite and crosscutting the Metzeral granite.

fracture zones that can measure several tens of meters in the vertical direction (Steinach). The most fractured outcrops are located near Andlau, where fracture density exceeds 10 fractures/m. Other authors have observed even higher fracture densities [86], most likely related to this site's location within the Lalaye-Lubine tectonic zone. This zone represents the boundary between the Saxo-Thurigian and Moldanubian domains [87], which extends under the graben and into the Black Forest near Baden-Baden (Figure 1(b)).

The predominant fracture set observed in outcrops and quarries is NW-SE. It is present at all sites except at Wolfbrünnen, where the quarry wall has almost the same orientation, and in Wald-Michelbach, where only five measurements are available (Figure 6). The conjugate set oriented NE-SW is present along with the NW-SE set at the same sites, except at Metzeral and Steinach, but in these cases not many measurements are available (5 and 8, respectively) (Figure 6). Although not a main fracture set, the N-S fracture set is present at all sites except Andlau (Figure 6).

A fourth fracture set is oriented E-W, but this set was present at only two sites, at Saint Pierre Bois and Wolfbrünnen, where it is the dominant set (Figure 6).

In granite fractures, quartz is the dominant fill mineral identified in the field. Whereas macroscopic fillings are rare, microscopic observations of thin sections provided evidence of two major types of textures and fillings: (1) cataclastic texture associated with a few quartz and illite-like clays fillings (Figures 10(b), 10(c), and 11) and (2) fractures with fillings of quartz, illite-like clays, and carbonates (Figures 10(d) and 11).

Fillings of quartz, illite-like clays, and carbonates are observed in fractures affecting granite from the Waldhambach quarry, the Heidelberg well, and the Windstein outcrop. At these three sites, the basement consists of a biotite-amphibole monzogranite. Alteration of the fracture-free granite matrix is minor, marked by partial sericitization of plagioclase and partial to complete replacement of ferromagnesian minerals by a chlorite-illite-epidote assemblage. Fractured granite samples are crosscut by NE-SW and NW-SE thin polyphase fractures.

The Weiler, Andlau, Wintzenheim, Metzeral, and Weinheim outcrops and Saint Pierre Bois, Steinach, Ottenhöffen, Wolfbrünnen quarries are predominantly biotite granite. Alteration of the granite matrix, regardless of fracture orientation, is marked by sericitization of plagioclase and muscovite and also to a certain extent by a complete breakdown of biotite/chlorite into illite-like clays and hematite. We distinguished two types of fractures: (1) fractures associated with cataclastic textures (Figures 10(a) and 10(b)) and (2) fractures without displacement and cataclasis (Figure 10(d)). Cohesive cataclasites are observed in NE-SW/NW-SE, E-W, and N-S structures (Figures 10(a)–

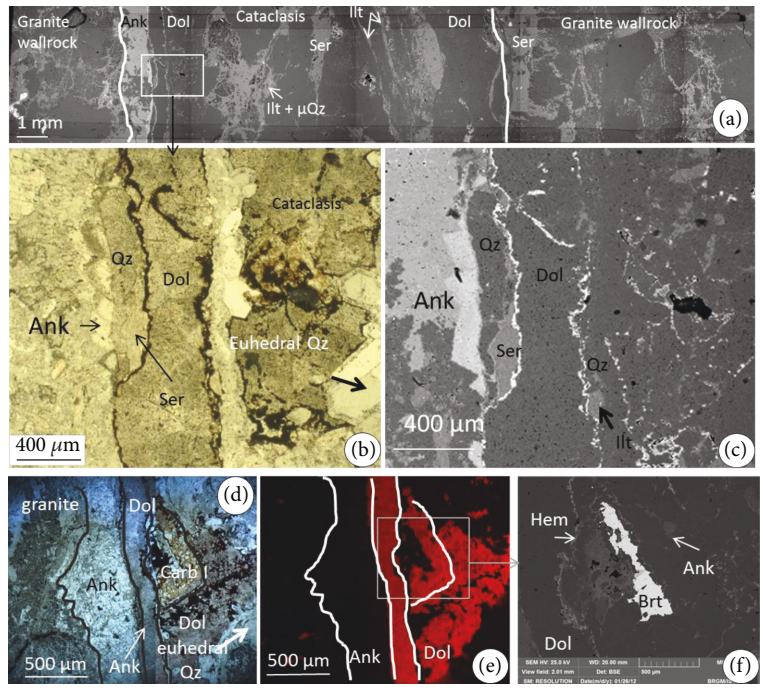

Figure 11: Polyphase filling in a microfracture that crosscuts the Waldhambach granite (images modified from [119]). (a) BSE image of the entire filling; (b) detail of textural relationships between cataclasis, euhedral quartz, and carbonates (dolomite and ankerite) (natural light); (c) the same zone in BSE; (d) detail showing the textural relationship between euhedral quartz, carbonates, and barite; (e) same image in CL: a first type of carbonates is red orange color under CL, and the second type is not luminescent (Ankerite); (f) same image in BSE.

10(d), respectively). Cohesive cataclasites are partially to totally cemented by an assemblage of microquartz and illite-like clays (Figure 10). In NE-SW and NW-SE structures at Ottenhoffen, veinlets of euhedral quartz have reworked cataclasites. Fractures without displacement that are filled with radial illite-like clays ± quartz or carbonates + quartz are everywhere observed in parts of the granite that have been preserved from direct weathering by meteoric waters (Figure 10(d)). Most of them are <200 μm fractures not visible in the outcrop; in thin sections, they are present as a network of fissures rather than as isolated fractures. For this reason, it was often difficult to measure their orientation. Only well-preserved fissures filled with radial illite-like clays are oriented at around N170°E in the Metzeral granite (Figure 10(d)).

At Waldhambach, details on a cm-thick fracture zone (Figure 11) provide evidence of polyphase filling very similar to that described in the EPS1 sample at 1427.30 m. The paragenetic sequence is defined by (1) cohesive cataclasite cemented by illite-like clays and microquartz and rimmed by massive oriented sericite (Figure 11(a)), (2) growth of euhedral quartz in the porosity of the cataclasite (Figures 11(b) and 11(c)), and (3) carbonates and finally barite (Figures 11(d)–11(f)). CL observations of carbonates show two types of carbonates: a first filling, which appears as red-orange color, and a second one that is not luminescent. Alteration of the fracture wall rocks is marked by intense sericitization of plagioclase, partial recrystallization of muscovite flakes in the sericite, and complete replacement of ferro-magnesian minerals by sericite, titanium oxides, and iron oxides (hematite).

5.3. Chemical Composition of Minerals in Cement. The electron microprobe was used to analyze feldspar in granites and in sandstones to trace the source of Ba that was precipitated from hydrothermal fluids (Supplementary Materials (available here)). Primary K-feldspar in granite and detrital K-feldspar in sandstones contain traces of Ba (1361–9538 mg.kg^{-1}). Rare authigenic K-feldspar does not contain Ba.

A few infrared spectra were acquired on bulk rock samples of altered granites and sandstones. Electron microprobe analyses were carried out on clay minerals observed in studied fractures that crosscut EPS1 and the Waldhambach granite and in studied EPS1 Buntsandstein sandstones and Permian arkoses of Saint Pierre Bois, to identify major clay minerals (Supplementary Materials). Infrared provides evidence of illite as a major alteration product in granites from Ottenhoffen, Wolfbrunnen, Wald-Michelbach and as a major clay mineral in the Hochburg sandstone. Most illite-like clays observed in thin sections are illite or illite-muscovite, according the triangular 4 Si-(Na + K + 2Ca)-(Mg + Fe^{2+}) diagram of Meunier and Velde [88] (Figure 12(a)).

Electron microprobe analyses were conducted on the different types of carbonates identified by CL (Supplementary Materials; Figure 12(b)). Carbonates that fill fractures in granites in the EPS1 well (EPS1-1427 m) and at

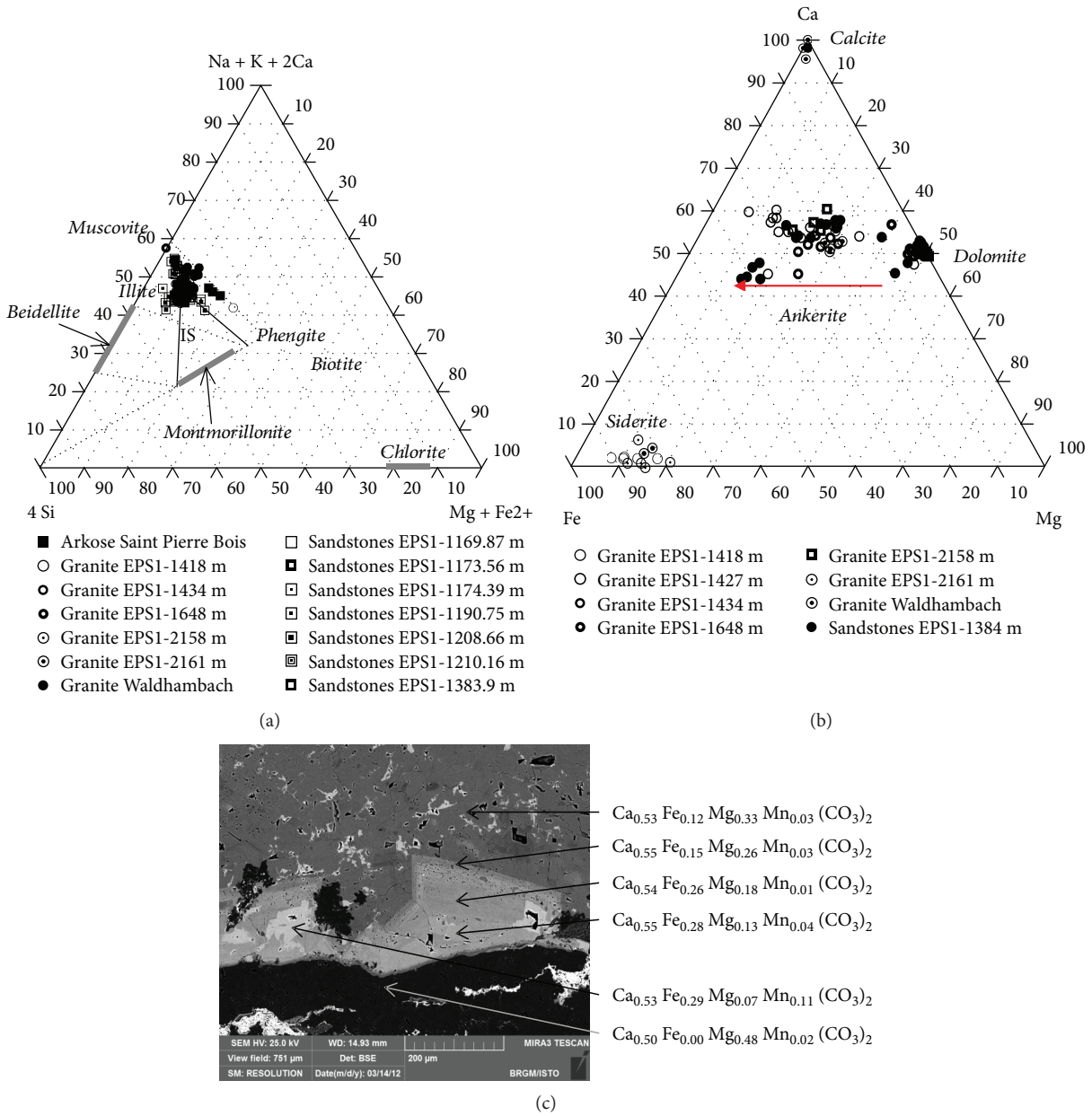

Figure 12: (a) Triangular 4 Si-(Na + K + 2Ca)-(Mg + Fe^{2+}) diagram of Meunier and Velde [94] showing the nature of the illite-like clays present in fractures of granites (EPS1 and Walhambach) and in sandstones. (b) Triangular Fe-Ca-Mg diagram showing chemical compositions of the various generations of carbonates in fractures of granites (EPS1 and Waldhambach) and in EPS1 sandstones. (c) Backscattered electron image showing chemical zoning of the dolomite-ankerite-kutnahorite solid solution (EPS1-1427 m).

Waldhambach and carbonates that cement sandstones in the EPS1 well (EPS1-1983.9 m) have an essentially homogeneous red-orange color under CL. This carbonate population is a quite pure dolomite (Dol). Dark red to nonluminescent carbonates consist of a dolomite-ankerite-kutnahorite solid solution with variable amounts of Fe (up to 24.70 wt % FeO) and Mn (up to 8.3 wt % MnO) substituting for Mg (Figure 12(c)). The luminescence of these carbonates decreases with increasing Fe and Mn in the crystal lattice. Fibrous carbonates present in biotite sheets in granite are essentially siderite that contains up to 3.5 wt % of CaO and up to 7.7 wt % of MgO. Calcite, which is yellow orange under CL, is observed in plagioclase alteration products and in some veinlets of EPS1-1648 m, EPS1-2158 m, and EPS1-2161 m.

5.4. Stable Isotopes. To determine the origins of the hydrothermal fluids, we analyzed the stable isotopes in the major minerals (carbonates, quartz, and barite) that fill both fractures and porosity in a few samples of sandstones, granites, and Permian volcanics from the EPS1 well and from quarry outcrops (Saint Pierre Bois, Waldhambach). Fractures with polyphase filling and relatively thick fractures were selected for this analytical task, but the number of selected samples

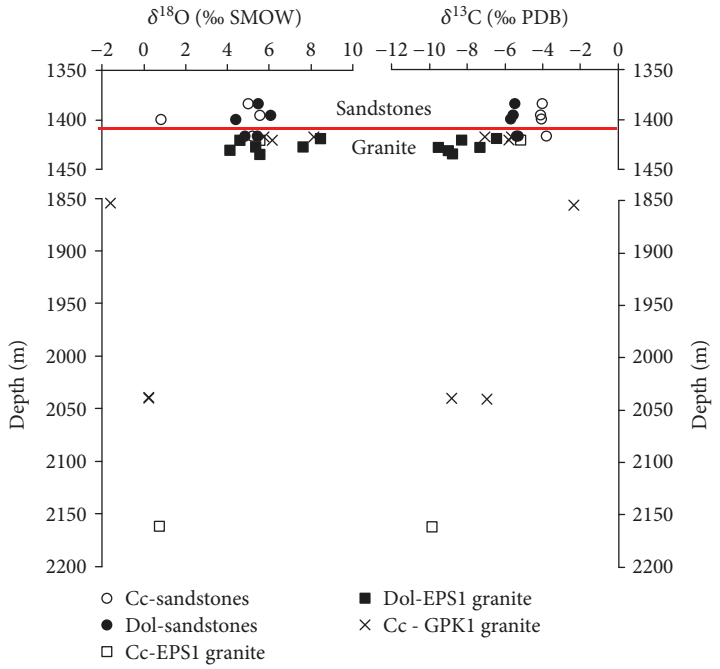

FIGURE 13: Profiles of $\delta^{18}O_{fluid}$ and $\delta^{13}C_{fluid}$ reported as a function of depth. The fluid data are calculated at equilibrium with calcite and dolomite in the upper part of the granite and the sandstones from the EPS1 well.

was limited due to the rarity of this type of sample. (C, O, and Sr) stable isotopes were measured on the primary carbonates (calcite and dolomite); oxygen isotopes were measured on quartz, and strontium isotopes on barite (Supplementary Materials).

The $\delta^{18}O$ values of dolomite in sandstones from the EPS1 well are almost homogeneous, ranging between +19.2 and +20.3‰$_{SMOW}$. Associated calcite, when present in the same samples, shows two populations of $\delta^{18}O$ values: (1) a value of +13.9 and (2) values of between +18.0 and +18.6‰$_{SsMOW}$. Oxygen isotopic fractionation between dolomite and calcite calculated for each sample is 5.3 between dolomite and the first population of calcite, and 2.0-2.3 between dolomite and calcite of the second population. Based on the oxygen isotopic fractionation of Sheppard and Schwarz [89], a value of 5.3 does not correspond to a consistent temperature, indicating that the first population of calcite and dolomite did not precipitate from the same fluid. On the contrary, values of 2.0-2.3 correspond to coherent temperatures of 135-160°C, indicating that dolomite and the second population of calcite precipitated from the same fluid at temperatures of 135-160°C. This temperature range is consistent with those obtained by fluid inclusion microthermometry in quartz and carbonates in veins in the EPS1 granite [67].

Fracture-fill dolomite in the first fracture interval in the upper part of the granite in the EPS1 well has homogeneous $\delta^{18}O$ values of 19.0-23.3‰$_{SMOW}$. Calcite from this interval has a similar $\delta^{18}O$ value of +18.6‰$_{SMOW}$, whereas calcite from the third fracture interval has a lower $\delta^{18}O$ value of 13.9‰$_{SMOW}$.

The $\delta^{18}O$ of euhedral quartz measured in fractures with polyphase filling that crosscuts granite in the EPS1 well at 1427.30 m and granite at Waldhambach are almost similar: +10.9 to +14.7‰ with an average value of +13.0 ± 2.1‰, and +11.6 to +14.8‰ with an average value of +13.0 ± 1.1‰, respectively.

The $\delta^{18}O$ of fluids were calculated at equilibrium with the various minerals in fractures that crosscut granite or fill porosity in the Buntsandstein, taking into account their formation temperature and fluid-mineral isotopic fractionations (for oxygen: quartz-H_2O [90]; dolomite-H_2O [91]; calcite-H_2O [92]; for carbon: dolomite-CO_2 [93]; calcite-CO_2 [94]). We used temperatures of 135-160°C obtained by calcite-dolomite oxygen thermometry for carbonate cements in sandstones from the EPS1 well. For quartz and carbonates filling fractures in granite from the EPS1 well, we used temperatures of 140-150°C according to [67] and complementary fluid inclusion microthermometry conducted on euhedral quartz in a polyphase vein of the EPS1 well, sample at -1427.3 m (Supplementary Materials). Taking into account the similarities of the polyphase fracture filling in the EPS1 granite at 1427.3 m and in the Waldhambach granite (same sequence of cementation in vein, same range $\delta^{18}O$ of quartz, and same range of $^{87}Sr/^{86}Sr$ in dolomite), we assume temperatures of 140-150°C for the quartz and carbonates filling the fracture in the Waldhambach granite.

The $\delta^{18}O$ and $\delta^{13}C$ values of the fluids (noted $\delta^{18}O_{fluid}$ and $\delta^{13}C_{fluid}$) at equilibrium with calcite and dolomite in the upper part of the granite and the sandstones from the EPS1 well are reported in Figure 13. The ranges of $\delta^{18}O_{fluid}$ at equilibrium with EPS1 dolomite in sandstones (4.4-6.1‰$_{SMOW}$) and granite (4.1 and 8.5‰$_{SMOW}$) and with a population of calcite in sandstone (5.0-5.2‰$_{SMOW}$) are almost identical; this range of $\delta^{18}O_{fluid}$ values indicates a major brine component in hydrothermal fluids. The $\delta^{18}O$ values of the fluids at equilibrium with the second

population of calcite (0.8‰$_{SMOW}$) and with a euhedral quartz-filled fracture that crosscuts the upper part of the granite in the EPS1 well (-6.3 and -0.9‰$_{SMOW}$) and at Walhambach (- 5.7 to -2.5‰$_{SMOW}$) are significantly lower and provide evidence of brines with variable amounts of meteoric component.

The $\delta^{13}C_{fluid}$ at equilibrium with EPS1 calcite (-4.1 to -3.8‰$_{PDB}$) and dolomite (-5.7 to -5.3‰$_{PDB}$) in sandstones are very similar to $\delta^{13}C_{fluid}$ at equilibrium with EPS1 calcite (-5.2‰$_{PDB}$) and dolomite (-6.5‰$_{PDB}$) in granite at the interface. The $\delta^{13}C_{fluid}$ at equilibrium with EPS1 carbonates in granite decrease down to -10‰$_{PDB}$ with depth. This wide range of $\delta^{13}C_{fluid}$ suggests mixing between different carbon sources: (1) carbon derived from carbonates present in the sedimentary cover (sandstones: $\delta^{13}C_{fluid}$ ~-4‰$_{PDB}$) (2) and carbon of deep-seated origin ($\delta^{13}C_{fluid}$~-10‰$_{PDB}$).

$^{87}Sr/^{86}Sr$ ratios measured in carbonates and barite that fill fractures are representative of the fluid signature at the moment of mineral precipitation. Dolomite and barite that fill a fracture that crosscuts Permian sandstones and volcanics in the Waldhambach quarry have $^{87}Sr/^{86}Sr$ ratios of 0.709817 and 0.709753, respectively. Dolomite that fills a fracture that crosscuts granite in the Walhambach granite has a $^{87}Sr/^{86}Sr$ ratio of 0.708993. The $^{87}Sr/^{86}Sr$ ratio of dolomite that fills a crosscutting fracture in granite in the EPS1 well is 0.708685. The close similarities of $^{87}Sr/^{86}Sr$ ratios of dolomite and barite in the Permian cover, in the Waldhambach granite, and in the EPS1 well suggest that dolomite and barite precipitated from the same hydrothermal fluids circulating at the cover/granite interface. Barite in crosscutting fractures in granite at Saint Pierre Bois has a $^{87}Sr/^{86}Sr$ ratio of 0.716273, providing evidence that barite was precipitated from a different fluid circulation than at Waldhambach and in the EPS1 well.

6. Discussion

6.1. Major Fracture Sets and Their Ages. The Rhine graben has a long tectonic history beginning with the Hercynian orogeny, followed by peneplanation with Permian N-S extension and sedimentation during a lengthy period of tectonic quiescence from the Triassic to the Jurassic. The region was uplifted during the Cretaceous; the Rhine graben began to open during the Eo-Oligocene and continued with different phases throughout the Tertiary [43, 48].

Three major fracture sets were identified in the sedimentary cover and the Hercynian basement of the Rhine graben: N-S, NE-SW/NW-SE, and E-W. In spite of the long history of the Rhine graben and the reactivation of numerous fractures and faults, especially in the basement, we can associate these main fracture sets with the tectonic phases of the Rhine graben area (Figure 3).

The N-S set is associated with the main graben phases of Eocene N-S compression and Oligocene E-W extension [48]. However, in the Hercynian basement, this set was reactivated during the Carboniferous Sudete phase [44]. This fracture set predominates in the Hercynian basement inside the graben (EPS1 well), but is minor on outcrops of Hercynian basement on the flanks of the Rhine graben. Andlau is an exception, where the NE-SW Lalaye-Lubine-Baden-Baden tectonic zone has a major impact on the surrounding area and the N-S fracture set may be hidden by this tectonic structure. In the Permo-Triassic sandstones, the main fracture set orientations fall between N160°E and N40°E similar to the orientation of large mapped structures genetically related to graben opening. The direction variation depends on the proximity of observation sites to major faults. Several N-S fractures are large fault zones in the Permo-Triassic sandstones both outside the Rhine graben (Bühl sandstones) and inside the Rhine graben (fault zone between 1172 and 1210 m in the EPS1 well).

The NE-SW and NW-SE fracture sets are well represented in granite outcrops on both sides of the Rhine graben and less so in the Hercynian granite in the EPS1 well within the Rhine graben. These NW-SE and NE-SW sets in the Hercynian basement are linked to Carboniferous N-S compression that was probably reactivated in the Tertiary. The NW-SE fracture set is also present in the Permo-Triassic sandstones and is probably linked with the most recent Plio-Quaternary NW-SE compression.

The E-W fracture set is primarily observed in the Hercynian basement at Saint Pierre Bois and Wolfbrünnen (this study) and at Schauenburg near Heidelberg on the eastern flank of the Rhine graben [73] and more rarely inside the graben. Fractures belonging to this set are less frequent than fractures of other sets. The Saint Pierre Bois quarry is located in the Permian Villé Basin. This basin collapsed due to a weakness zone caused by the intersection of Lalaye-Lubine-Baden-Baden tectonic structure and the Sainte Marie aux Mines fault zone, which is oriented N30°E and crosscuts the entire southern Vosges Massif (Figure 1(b)). In this complex zone, the basement is highly fractured by N-S to E-W faults and a N130°E fault set [86, 95]. Another E-W fault also affects Permian rhyolites at Schauenburg [73]. The E-W set is linked to the most recent tectonic phases of the Hercynian stages during the Permian [46], which correspond to extension prior to the collapse of the range and peneplanation. These fractures were also reactivated by brittle deformation in the Tertiary [43].

6.2. Relation between Fracture Direction and Fracture Fillings. The combination of structural measurements and mineral sequences of fracture fillings provides evidence that some types of filling are associated preferentially with specific fracture set directions (Figure 14).

6.2.1. N-S Fracture Set. Outside the graben, N-S fractures are commonly observed in Permian-Triassic sandstones and less so in the Hercynian basement (Figures 4 and 6). Fractures generally exhibit shearing and cataclastic textures and are unfilled to poorly filled in both sandstones and Hercynian basement. Only a few fractures filled with radial illite crosscut Hercynian granite on the Metzeral outcrop. Sandstones exposed in quarries near major N-S features are highly fractured and bleached (Cleebourg, Bad Durkheim), and fillings are absent, suggesting that these N-S structures represent present-day fluid recharge zones. When fillings are present, cements are dominantly microquartz and illite

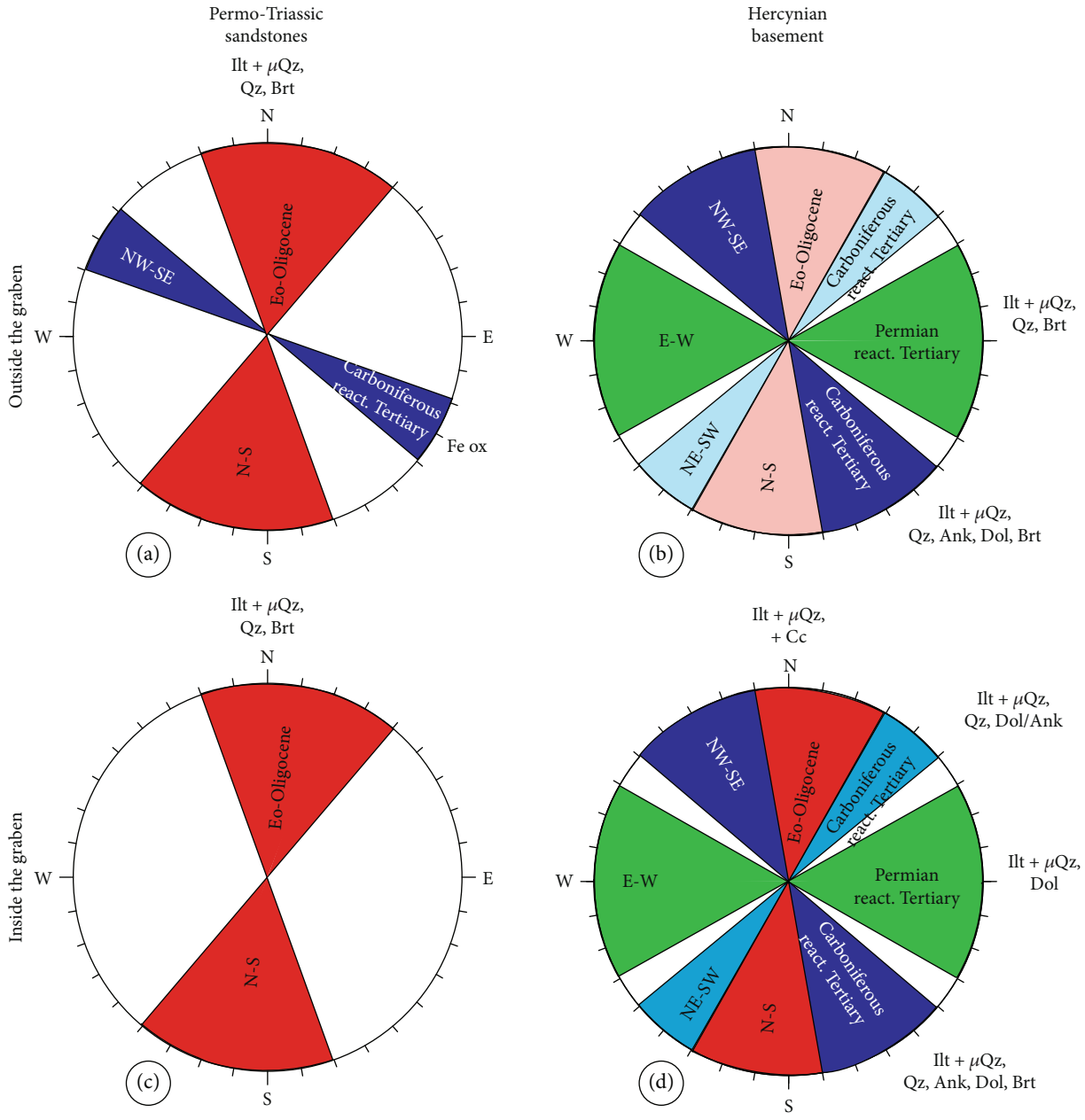

Figure 14: Synthesis of the main observed fracture directions with associated filling in the Hercynian granite and the Permo-Triassic sandstones inside and outside the graben. The Ilt + μQz combination is generally associated with cataclasis.

(Figure 14(a)). Rare quartz and/or barite veins reoccur within older cataclastic structures (Figure 14(a)). Microthermometric and oxygen isotopic data of this type of quartz in a N-S fault plane affecting Triassic sandstones at Bühl (130°C, $\delta^{18}O_{fluid}$ -1.5‰) [96] indicates that the quartz was precipitated from hot fluids composed of brines mixed with meteoric fluids. The discovery of such temperatures outside the graben indicates that these fillings formed at depth prior to graben collapse.

Inside the graben, the N-S fractures affect both the Triassic sandstones and the Hercynian basement (Figures 14(c) and 14(d)). The large fracture zone affecting Triassic sandstones at depths of 1170-1210 m is quite similar to the large fault plane at Bühl in terms of mineral fillings and formation conditions (Figures 14(a) and 14(c)). Unlike Hercynian granites outside the graben, N-S fractures in the EPS1 Hercynian granite inside the graben are filled with calcite (Figure 14(d)) precipitated from brines with a high meteoric water content ($\delta^{18}O_{fluid}$ ~0.8‰$_{SMOW}$) down to 600 m. Calcite with similar $\delta^{18}O$ was also found in the EPS1 sandstones (this study) and in granite in other wells (GPK1 at 1998.9 m; GPK2, GPK3, and GPK4 down to ~4900 m) [68, 97]. Dolomite is found only in the first and second fracture intervals of the EPS1 well corresponding to depths of 200-300 m under the cover/granite interface. Such data strongly suggest that brine that circulated at the cover/basement interface and

precipitated dolomite in ancient structures prior to graben collapse continued to circulate at higher depth into the granite via tertiary N-S structures. The lower $\delta^{18}O_{fluid}$ range seems to suggest an increasing supply of meteoric waters into the fractured reservoir.

6.2.2. NE-SW and NW-SE Fracture Sets. The NE-SW and NW-SE fracture sets are primarily present in the Hercynian basement inside and outside the Rhine graben (Figures 14(b) and 14(d)).

Numerous fractures within the NE-SW and NW-SE fracture sets have polyphase fillings. This indicates that (1) various generations of fluids used these fracture sets and (2) some of this circulation occurred prior to graben collapse. The more complex polyphase filling consists of cohesive cataclasites cemented by early illite and microquartz, followed by euhedral quartz and a late stage composed of dominant dolomite, minor ankerite, and calcite (Figures 14(b) and 14(d)). The variability of the mineral fillings is representative of changes of fluid chemical composition over time. Fluid inclusion microthermometric and oxygen isotopic data available on the various mineral fillings in fractures crosscutting granite and in matrix cementing sandstones at the cover/basement transition make it possible to determine fluid origins and minimal formation temperatures:

(i) Quartz in granite in the EPS1 well precipitated from multiple generations of NaCl-$MgCl_2$/$CaCl_2$-rich fluids at about 140-150°C [67, 69, 74]. The highest temperatures reached values up to 200°C [67]. Quartz in granite at Waldhambach shows similar characteristics. The $\delta^{18}O_{fluid}$ (-6.3 to -0.9‰) deduced from this quartz provides evidence of brines mixed with variable amounts of meteoric waters

(ii) Dolomite in sandstones in the EPS1 well precipitated from brines at temperatures of about 135-160°C and with $\delta^{18}O_{fluid}$ of 4.4 to 6.1‰, and $\delta^{13}C_{fluid}$ of -5.7 to -5.3‰.

(iii) Dolomite in granite in the EPS1 well precipitated from brines at about 140-150°C [67, 69, 74, 98]. Dolomite in the Waldhambach granite shows similar characteristics. The $\delta^{18}O_{fluid}$ (4.4 to 8.5‰) and $\delta^{13}C_{fluid}$ (-9.0 to -6.5‰) deduced from dolomite indicate brine fluids with minor meteoric waters. The lower $\delta^{13}C_{fluid}$ values are due to the contribution of deep-seated carbon

(iv) Barite at the roof of the EPS1 granite also provide evidence of brines (with up to 23 wt% Eq NaCl) and formation temperatures of ~130°C [69, 99]

As the data demonstrates, all the fill minerals precipitated at depth within a narrow temperature range (130-150°C). The $\delta^{18}O_{fluid}$ variations provide evidence of hot brines mixed with variable amounts of meteoric waters. The origins of these brines are probably seawater-modified fluids or fluids equilibrated with Triassic evaporates as proposed by [67, 98]. Carbonates and barite precipitated from brines mixed with a minor eteoric water component. The $\delta^{13}C_{fluid}$ provides evidence of two sources: carbon derived from carbonates present in the sedimentary cover (sandstones: $\delta^{13}C_{fluid}$ ~-4‰$_{PDB}$) and carbon of deep-seated origin ($\delta^{13}C_{fluid}$ ~-9‰$_{PDB}$). These $\delta^{13}C_{CO2}$ deduced from dolomite are consistent with the $\delta^{13}C$ of CO_2 trapped in magmatic quartz in granite analyzed at different depths of the EPS1 well [100]. The range of carbonate chemistry (from pure dolomite to ankerite and siderite) and barite deposition are probably represent variable water/rock interactions between brines, Fe-Mg minerals (Fe, Mg, and Mn release), and feldspars (plagioclase: Ca release; K-feldspar: Ba release) from granite and sandstones. The distribution of dolomite/ankerite with minor barite filling in NE-SW and NW-SE fractures of the granite roof and in residual porosity in the sandstones of the EPS1 well helps define the scale of brine circulation at the cover/granite interface from the top of the sandstones down to 200-300 m into the granite. The same information is inferred from very similar low $^{87}Sr/^{86}Sr$ ratios (~0.7089-0.7098) measured in dolomite in the Waldhambach granite and overlying Permian volcanic rocks.

Unlike carbonates and barite, quartz and associated illite likely precipitated from fluids with a high meteoric water component, in agreement as described by [101]. The silica source was probably the partial dissolution of feldspars, whereas illite was an alteration product of feldspars and primary micas at 130-200°C.

6.2.3. E-W Fracture Set. Outside the graben, fractures belonging to the E-W fracture set observed in granites at Saint Pierre Bois, Wolfbrunnen (this study), and at Schauenburg [73] consist of cohesive cataclasites cemented by microquartz and illite. Euhedral quartz and barite crosscut these cataclasites in a few locations at Saint Pierre Bois (Figure 14(b)). The $^{87}Sr/^{86}Sr$ ratio of barite (~0.716) at Saint Pierre Bois is significantly higher than the $^{87}Sr/^{86}Sr$ ratio of barite that fills NW-SE fractures, indicating that they precipitated from different fluids and probably at different times. U-Th data on the Schauenburg E-W cataclastic fault provide evidence that the early cataclasis zone acts as a current recharge conduit for surficial fluids [73].

Inside the graben, only a few EW fractures are encountered in the EPS1 well. One fracture at 1430 m has a polyphase filling, including early-filling microquartz + illite followed by quartz and dolomite (Figure 14(d)).

6.3. Paleocirculation, Tectonic History, and Present-Day Circulation. The comparison of major fracture sets, their mineral fillings, and their distribution in the overlying formations and in the Hercynian basement inside and outside the graben highlights different stages of deep hot fluid circulation at the cover/basement interface that has been active since graben formation until the present. Two major types of fillings precipitated successively from fluids over the same temperature range (about 130-150°C): (a) cohesive cataclasites cemented by silicates (quartz, illite) that precipitated from brines mixed with a high meteoric water component and (b) carbonates and barite that essentially precipitated from brines. It is noteworthy that both quartz/illite and

carbonates/barite cementation is present in the Hercynian NE-SW and NW-SE fracture set and in the N-S fracture set. However, they differ by the nature of the carbonate that precipitated (dolomite then calcite in Hercynian fractures inside and outside the graben, and calcite in N-S fractures in the graben), by the depth of carbonate precipitation in EPS1 granite fractures (200-300 m for dolomite and more than 600 m for calcite), and probably by their timing. From these data, at least four elements seem to determine the initiation of convection fluid cells at the graben scale: (1) introduction of meteoric waters, (2) temperature, (3) fracture directions, and (4) fluid chemistry.

Prior to graben formation, the maximum burial temperatures attained in Buntsandstein sandstones are those of Buntsandstein sandstones in the eastern part of the Paris Basin. These temperatures did not exceed 100°C, and a normal thermal gradient occurs [102, 103] thus making it impossible to reach the temperatures of approximately 130-150°C (up to 200°C) that are measured in fracture fill minerals in the Rhine graben [67]. Graben formation in the Tertiary favoured both (a) temperature conditions induced by an abnormal thermal gradient associated with volcanism [50] and (b) inflows of meteoric waters to the cover/basement interface via permeable faults that crosscut the entire thickness of the sedimentary cover down to the Hercynian basement [43, 44]. The first inflows of meteoric waters probably began during Eocene E-W compression [43, 48] first via the N-S structures (Figure 15(a)). Descending cold meteoric waters mobilized silica and increased rock permeability by alteration and dissolution of silicates such as feldspars. At the cover/basement interface, descending meteoric waters mix with upflowing hot brines through the porosity of the Permo-Triassic sandstones and via reactivated Permo-Carboniferous NE-SW and NW-SE structures, resulting in first illite/quartz cementation (stage 1; Figure 15(a)). Water influx and the high thermal gradient likely gave rise to the first convective cells of fluid circulation through the sedimentary-basement interface, favouring brine/rock interaction and leading to the earliest dolomite/barite cementation (stage 2; Figure 15(a)). During these stages, brine/rock ratios remain low, as the chemical variability of carbonates suggests.

Increasing volumes of meteoric waters penetrated into the graben during major E-W extension and the graben collapse phase of the Oligocene, via large approximately N-S faults and also reactivated older faults [48]. Descending cold meteoric waters continued to mobilize silica and increased rock permeability. Active subsidence and volcanic activity during this period, primarily occurring along the western border of the Rhine graben [50], maintained hydrothermal temperature conditions in the graben. Deposition processes involved during this period were the same as those involved in depositional stages 1 and 2 (stage 3 and 4; Figure 15(b)). With active convective circulation, fluids penetrated and altered to increasing depths into the Hercynian basement in the Rhine graben, as shown by the distribution of calcite deposits in the Soultz wells [56, 68, 97].

Today's thermal profiles to a depth of 5000 m in the Soultz-sous-Forêts wells show a convection cell in the Buntsandstein between 1000 and 3500 m in the granite [51, 104]. This convection is also present in the deep geothermal wells of Landau [105] and Rittershoffen [106], close to Soultz-sous-Forêts; it reaches the granite basement, and its basal depths are 3000 m and 2700 m, respectively. However, in the eastern part of the Rhine graben, in the geothermal wells of Bruchsal [107] and Basel [108], there appears to be no convective cell, even though the wells reach depths of 2500 m and 4680 m, respectively. At Soultz-sous-Forêts, circulation between wells has been identified primarily within the NE-SW and NW-SE fracture sets [54, 109]. Geochemical studies of geothermal brines produced in the Soultz-sous-Forêts, Rittershoffen, Landau, and Insheim (close to Landau) geothermal sites show high salinity values that indicate brines formed by heightened evaporation of seawater and low meteoric water content [110]. Moreover, the estimated geothermometers indicate an equilibrium temperature close to 225 ± 25°C at Soultz-sous-Forêts [111]. The geothermal fluids collected in the granite seem originate from Triassic sedimentary formations located at depths of more than 4 km. The formation is present at that depth in the northeastern part of the Rhine graben, where the basin is deepest. In this part, the eastern border fault of the graben is a major feature [112] and it penetrates deeper into the earth's crust [113]. Therefore, this may favour fluid penetration into the deeper part of the graben where they become mineralized at the contact with Permo-Triassic saline formations. Then, these fluids flow across the graben through the oblique NE-SW reactivated Hercynian fractures to mix with fresh meteoric waters coming from the western side of the graben (Figure 15(c)).

7. Conclusions

Examination of 20 outcrops including 16 quarries along the main border faults on both sides of the Rhine graben and analysis of cores from the EPS1 well drilled in the Rhine graben show that the Paleozoic basement and Permo-Triassic formations were affected by several phases of brittle tectonics associated with fluid circulation pulses.

The fillings of Hercynian fractures in the Paleozoic basement, oriented primarily NE-SW and NW-SE, are poly-phase. The first stage of infilling (stage 1) corresponds to a cataclastic phase associated with illite and quartz, followed by euhedral quartz infillings. The presence of this pattern in the Hercynian and Permian fracture sets, mainly observed in the EPS1 well and in the Waldhambach quarry, indicates that fluid circulation that caused these fillings occurred prior to graben opening. Stage 1 is characterized by (a) reactivation of ancient Hercynian structures at the beginning of graben opening during the early Eocene related to the N-S compression affecting the European platform and (b) the first major infiltration of meteoric fluids through the sedimentary cover into the Hercynian basement.

The second major stage (stage 2) is marked by dolomite deposition within tension fractures in the upper part of the Hercynian granite basement (first 200-300 m) and in sandstone porosity in the sedimentary cover. This stage is likely the result of convective circulation of deep hot brines mixed

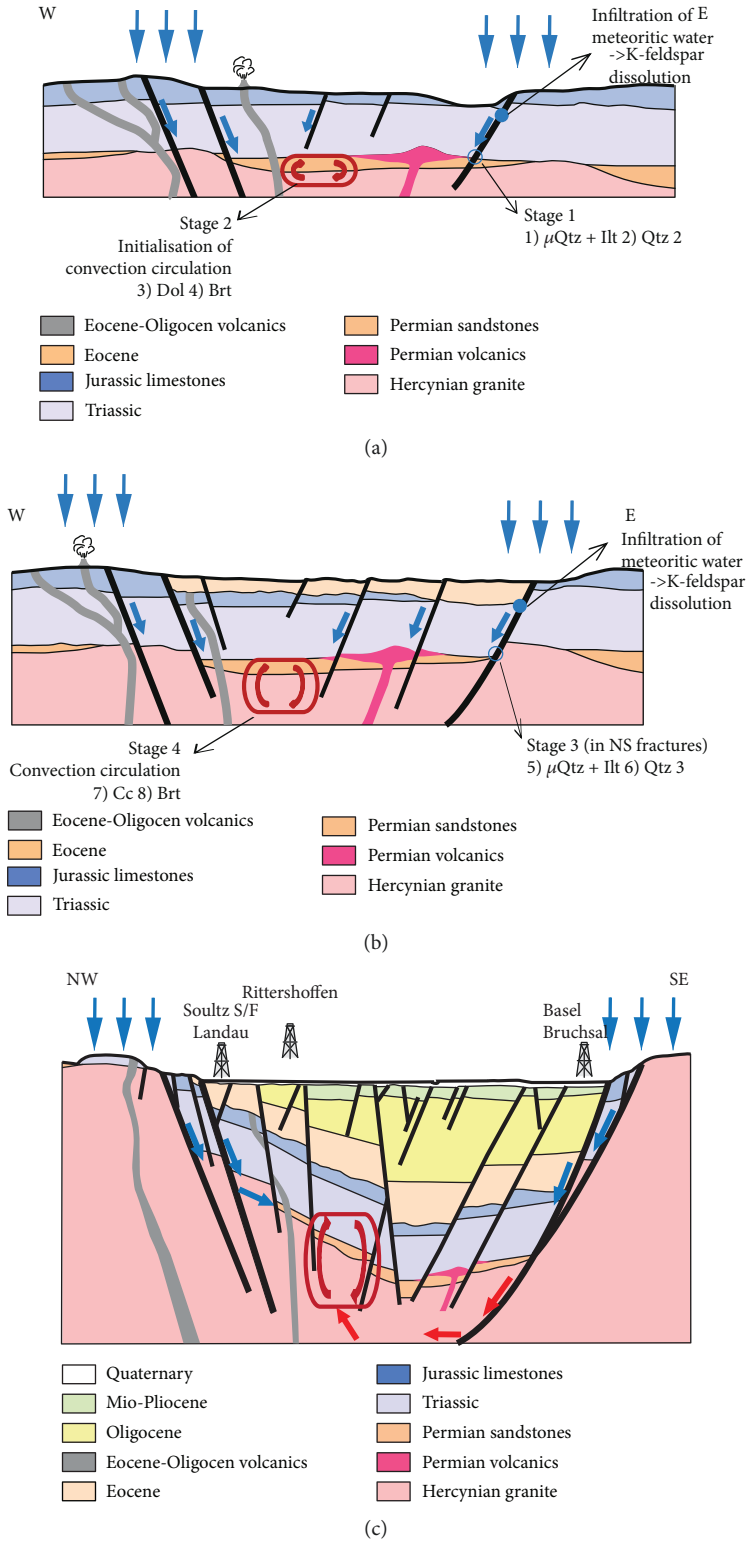

Figure 15: Schematic of fluid circulation and rock interaction during Tertiary tectonic episodes. (a) Early rifting stage during the Eocene under N-S compression associated with the paleofluid stages 1 and 2. (b) Lower Eocene and Oligocene rifting under E-W extension associated with paleofluid stages 3 and 4. (c) Present-day situation; location of geothermal sites is indicated as an approximate projection. Conceptual cross sections modified from Sittler (1992). Vertical scale is exaggerated. Blue arrows: meteoritic waters; red arrows: hot brines; curved arrows: convection cell. See explanation in the text.

with meteoric waters, probably initiated at the sedimentary cover/basement during the early stage of graben formation and associated with mantle diapirism and volcanism (Eocene-Oligocene).

A cataclasis stage is observed in the N-S fractures affecting the basement and also in Permo-Triassic sandstones, both within and outside the Rhine graben (stage 3). In outcrop, this fracture set shows few macroscopic mineralogical fillings, probably because fracture planes have been subjected to surface weathering alteration. However, at the microscopic scale, tension fissures in granite are observed to be filled with radial illite, and several large N-S shear zones affecting the Buntsandstein sandstones are filled with quartz associated with illite, hematite, and barite. Within the Rhine graben, similar quartz and barite fillings are identified in a major fracture network that affects the Buntsandstein sandstones, relatively far from the basement/cover interface. Stage 3 corresponds to the major stage of the graben opening linked with E-W extension during the Eocene-Oligocene and of a second major infiltration of meteoric fluids deeper into the Hercynian basement. Fracture fillings of this stage probably recorded fluid circulation associated with the graben opening stage just prior to and during uplift of the shoulders.

The fourth major stage (stage 4) is the continuation of convective circulation of deep hot brines mixed with meteoric-derived waters at the sedimentary cover/basement in the Rhine graben during and after the collapse. Stage 4, which is present only in the graben, is marked by barite filling N-S fractures in Buntsandstein sandstones and by calcite and barite also filling N-S fractures in the granite down to a depth of 4900 m in the Rhine graben. The Ca origin would be plagioclase dissolution and remobilization of ancient dolomite, whereas the Ba origin would be K-feldspar dissolution by descending meteoric waters. Calcite and barite continue to precipitate at depth today, and convective circulation extends deeper into the Hercynian granite basement.

To conclude, the reactivation of old Hercynian structures oriented NE-SW and NW-SE related to the earliest Eocene tectonic history of Tertiary graben formation has favoured the downflow of meteoric water and initiated fluid convection cells at the sedimentary cover-basement interface. This activity continued in the N-S structures during the Oligocene extensional phase. Today, these large N-S structures form recharge drains and promote a large-scale vertical convective circulation system in the western part of the basin, in the Buntsandstein, and in the Hercynian granitic basement.

Data Availability

The data used to support the findings of this study are available from the corresponding author upon request.

Conflicts of Interest

The authors declare that they have no conflicts of interest.

Acknowledgments

This work was funded by ADEME and BRGM within the framework of the TECITUR R&D project under agreement no. 1005C0140 and ANR under grant agreement ANR-15-CE06-0014 (Project CANTARE-Alsace). The authors thank the managers of the quarries and their associates for authorization to access the walls and site facilities. In particular, we would like to mention (i) Francine Loegel from LOEGEL for access and discussion at the Rothbach quarry; (ii) Jérémie de Bonneval and Sébastien Kuhn from LEONHART for access to the Saint Pierre Bois quarry; (iii) Willi Kuhn from GEBRUCHER KUHN for access to the Waldhambach quarry; (iv) RAUSCHER for access to the Cleebourg quarry; (v) FISHERGRANIT for access to the Wolfbrunnen quarry; and (vi) CARRIERE DE GRES DE CHAMPENAY for access to the Champenay quarry. We also thank Edgard Nitch and Wolfgang Werner from LGRB Freiburg for information about the quarries and mineralization in the Black Forest, and Albert Genter, vice general manager of ES-G, for access to the Soultz-sous-Forêts site and rock samples. For analytics, the authors thank Laurent Bailly (BRGM) for fluid inclusion microthermometry, Christine Flehoc (BRGM) for (C, O) stable isotopes, Catherine Guerrot (BRGM) for strontium isotopes, Andrey Gurenko (CRPG Nancy) for ionic probe analyses, and Guillaume Wille (BRGM) for electron microprobe and SEM images. Finally, we are also grateful to Prof. Andrea Moscariello (Universty of Geneva) for their useful comments and recommendations, which greatly improved this manuscript.

Supplementary Materials

EPS1_Cores_Sandstones: fracture orientation data on Buntsandstein EPS1 well cores. EPS1_Cores_Granite: fracture orientation data on Paleozoic granite EPS1 well cores. Outcrops-Quarries_Sandstones: fracture orientation data on Buntsandstein in outcrops and quarries. Outcrops-Quarries_Basement: fracture orientation data on Paleozoic basement in outcrops and quarries. Infrared data: on samples from Ottenhöffen, Wolfbrunnen, Wald-Michelbach, Hochburg. EPMA on feldspar: on Buntsandstein sandstone sample from the EPS1 well and Paleozoic granite sample from Waldhambach. EPMA on carbonates: on Buntsandstein sandstone and Paleozoic granite samples from EPS1 well and Paleozoic granite sample from the Waldhambach. EPMA on barite EPS1: on Buntsandstein sandstone samples from the EPS1 well. EPMA on clay minerals: on Stephanian arkose sample from Saint Pierre Bois, Paleozoic granite sample from Waldhambach, and Buntsandstein sandstone and Paleozoic granite samples from the EPS1 well. Isotopic data: on samples from Saint Pierre Bois, Steinach, Waldhambach, EPS1 well (this study), and GPK1 well [98]. *(Supplementary Materials)*

References

[1] C. E. Manning and S. E. Ingebritsen, "Permeability of the continental crust: implications of geothermal data and

metamorphic systems," *Reviews of Geophysics*, vol. 37, no. 1, pp. 127–150, 1999.

[2] C. A. J. Wibberley, G. Yielding, and G. Di Toro, "Recent advances in the understanding of fault zone internal structure: a review," *Geological Society, London, Special Publications*, vol. 299, no. 1, pp. 5–33, 2008.

[3] F. Mazzarini, I. Isola, G. Ruggieri, and C. Boschi, "Fluid circulation in the upper brittle crust: thickness distribution, hydraulic transmissivity fluid inclusion and isotopic data of veins hosted in the Oligocene sandstones of the Macigno Formation in southern Tuscany, Italy," *Tectonophysics*, vol. 493, no. 1-2, pp. 118–138, 2010.

[4] K. Bucher and I. Stober, "Fluids in the upper continental crust," *Geofluids*, vol. 10, 253 pages, 2010.

[5] D. L. Siler and B. M. Kennedy, "Regional crustal-scale structures as conduits for deep geothermal upflow," *Geothermics*, vol. 59, pp. 27–37, 2016.

[6] P. Robert, "Histoire géothermique et diagenèse organique," in *Bulletin des Centres de Recherches Exploration-Production Elf Aquitaine*, p. 345, Elf Aquitaine, 1985.

[7] F. Pirajno and M. Santosh, "Mantle plumes, supercontinents, intracontinental rifting and mineral systems," *Precambrian Research*, vol. 259, pp. 243–261, 2015.

[8] A. Aydin, "Fractures, faults, and hydrocarbon entrapment, migration and flow," *Marine and Petroleum Geology*, vol. 17, no. 7, pp. 797–814, 2000.

[9] A.-M. Boullier, K. Fujimoto, T. Ohtani et al., "Textural evidence for recent co-seismic circulation of fluids in the Nojima fault zone, Awaji island, Japan," *Tectonophysics*, vol. 378, no. 3-4, pp. 165–181, 2004.

[10] O. Dauteil and L. E. Ricou, "Une circulation de fluides de haute-température à l'origine du métamorphisme crétacé nord-pyrénéen," *Geodinamica Acta*, vol. 3, no. 3, pp. 237–249, 1989.

[11] N. H. S. Oliver, "Review and classification of structural controls on fluid flow during regional metamorphism," *Journal of Metamorphic Geology*, vol. 14, no. 4, pp. 477–492, 1996.

[12] P. Boulvais, "Fluid generation in the Boucheville Basin as a consequence of the North Pyrenean metamorphism," *Comptes Rendus Geoscience*, vol. 348, no. 3-4, pp. 301–311, 2016.

[13] D. R. Faulkner, C. A. L. Jackson, R. J. Lunn et al., "A review of recent developments concerning the structure, mechanics and fluid flow properties of fault zones," *Journal of Structural Geology*, vol. 32, no. 11, pp. 1557–1575, 2010.

[14] V. F. Bense, T. Gleeson, S. E. Loveless, O. Bour, and J. Scibek, "Fault zone hydrogeology," *Earth-Science Reviews*, vol. 127, pp. 171–192, 2013.

[15] R. H. Sibson, "Structural permeability of fluid-driven fault-fracture meshes," *Journal of Structural Geology*, vol. 18, no. 8, pp. 1031–1042, 1996.

[16] J. V. Rowland and S. F. Simmons, "Hydrologic, magmatic, and tectonic controls on hydrothermal flow, Taupo volcanic zone, New Zealand: implications for the formation of epithermal vein deposits," *Economic Geology*, vol. 107, no. 3, pp. 427–457, 2012.

[17] S. F. Cox, "The application of failure mode diagrams for exploring the roles of fluid pressure and stress states in controlling styles of fracture-controlled permeability enhancement in faults and shear zones," *Geofluids*, vol. 10, pp. 217–233, 2010.

[18] K. C. Condie, *Plate Tectonics & Crustal Evolution*, Butterworth-Heinemann, 4th edition, 1997.

[19] J. Meixner, E. Schill, J. C. Grimmer, E. Gaucher, T. Kohl, and P. Klingler, "Structural control of geothermal reservoirs in extensional tectonic settings: an example from the Upper Rhine Graben," *Journal of Structural Geology*, vol. 82, pp. 1–15, 2016.

[20] P. A. Ziegler, "European Cenozoic rift system," *Tectonophysics*, vol. 208, no. 1-3, pp. 91–111, 1992.

[21] A. Gerard and O. Kappelmeyer, "The Soultz-sous-Forets project," *Geothermics*, vol. 16, no. 4, pp. 393–399, 1987.

[22] C. Clauser, E. Griesshaber, and H. J. Neugebauer, "Decoupled thermal and mantle helium anomalies: implications for the transport regime in continental rift zones," *Journal of Geophysical Research: Solid Earth*, vol. 107, no. B11, 2002.

[23] L. Rybach, "The geothermal conditions in the Rhine Graben - a summary," *Bulletin für Angewandte Geologie*, vol. 12, pp. 29–32, 2007.

[24] E. Roulleau, F. Bravo, D. L. Pinti et al., "Structural controls on fluid circulation at the Caviahue-Copahue Volcanic Complex (CCVC) geothermal area (Chile-Argentina), revealed by soil CO_2 and temperature, self-potential, and helium isotopes," *Journal of Volcanology and Geothermal Research*, vol. 341, pp. 104–118, 2017.

[25] M. Zucchi, A. Brogi, D. Liotta et al., "Permeability and hydraulic conductivity of faulted micaschist in the eastern Elba Island exhumed geothermal system (Tyrrhenian sea, Italy): insights from Cala Stagnone," *Geothermics*, vol. 70, pp. 125–145, 2017.

[26] A. M. Schleicher, L. N. Warr, and B. A. van der Pluijm, "Fluid focusing and back-reactions in the uplifted shoulder of the Rhine rift system: a clay mineral study along the Schauenburg Fault zone (Heidelberg, Germany)," *International Journal of Earth Sciences*, vol. 95, no. 1, pp. 19–33, 2006.

[27] T. Abebe, *Geological Limitations of a Geothermal System in a Continental Rift Zone: Example the Ethiopian Rift Valley*, World Geothermal Congress, Kyushu-Tohoku, Japan, 2000.

[28] C. Lampe, M. Person, S. Nöth, and W. Ricken, "Episodic fluid flow within continental rift basins: some insights from field data and mathematical models of the Rhinegraben," *Geofluids*, vol. 1, no. 1, 52 pages, 2001.

[29] C. Lampe and M. Person, "Advective cooling within sedimentary rift basins—application to the Upper Rhinegraben (Germany)," *Marine and Petroleum Geology*, vol. 19, no. 3, pp. 361–375, 2002.

[30] H. Dresmann, N. Keulen, Z. Timar-Geng, B. Fügenschuh, A. Wetzel, and H. Stünitz, "The south-western Black Forest and the Upper Rhine Graben Main Border Fault: thermal history and hydrothermal fluid flow," *International Journal of Earth Sciences*, vol. 99, no. 2, pp. 285–297, 2010.

[31] C. Giersch, "Thermohydrodraulik des kristallinen Grundgebirges am Beispiel des östlichen Oberrheingrabens," *AGK Schriftenr*, vol. 72, pp. 1–156, 2006.

[32] J.-B. Edel and K. Schulmann, "Geophysical constraints and model of the Saxothuringian and Rhenohercynian subductions –magmatic arc system in NE France and SW Germany," *Bulletin de la Societe Geologique de France*, vol. 180, no. 6, pp. 545–558, 2009.

[33] J. B. Edel and K. Weber, "Cadomian terranes, wrench faulting and thrusting in the Central Europe Variscides: geophysical

and geological evidence," *Geologische Rundschau*, vol. 84, no. 2, pp. 412–432, 1995.

[34] P. A. Ziegler, "Geodynamic model for the paleozoic crustal consolidation of western and central europe," *Tectonophysics*, vol. 126, no. 2-4, pp. 303–328, 1986.

[35] P. Matte, "Tectonics and plate tectonics model for the Variscan belt of Europe," *Tectonophysics*, vol. 126, no. 2-4, pp. 329–374, 1986.

[36] O. Oncken, C. von Winterfeld, and U. Dittmar, "Accretion of a rifted passive margin : the Late Paleozoic Rhenohercynian fold and thrust belt (Middle European Variscides)," *Tectonics*, vol. 18, no. 1, pp. 75–91, 1999.

[37] C. Schneider, *Les granitoïdes de la partie Nors-Est des Vosges moldanubiennes: evolutions magmatique et structural. [PhD thesis of Strasbourg University]*, Strasbourg, France, 1984.

[38] T. Villemin, F. Alvarez, and J. S. Angelier, "The Rhinegraben: extension, subsidence and shoulder uplift," *Tectonophysics*, vol. 128, no. 1-2, pp. 47–59, 1986.

[39] R. Altherr, U. Henes-Klaiber, E. Hegner, M. Satir, and C. Langer, "Plutonism in the Variscan Odenwald (Germany): from subduction to collision," *International Journal of Earth Sciences*, vol. 88, no. 3, pp. 422–443, 1999.

[40] R. Altherr, A. Holl, E. Hegner, C. Langer, and H. Kreuzer, "High-potassium, calcalkaline I-type plutonism in the european variscides: northern vosges (France) and northern schwarzwald (Germany)," *Lithos*, vol. 50, no. 1-3, pp. 51–73, 2000.

[41] G. H. Eisbacher, E. Lüschen, and F. Wickert, "Crustal-scale thursting and extension in the Hercynian Schwartzwald and Vosges Central Europe," *Tectonics*, vol. 8, no. 1, pp. 1–21, 1989.

[42] S. Roussé, *Architecture et dynamique des séries marines et continentales de l'Oligocène moyen et supérieur du sud du Fossé rhénan: évolution des milieux de dépôt en contexte de rift en marge de l'avant pays alpin*, Doctoral dissertation, Strasbourg 1, 2006.

[43] M. E. Schumacher, "Upper Rhine Graben: Role of preexisting structures during rift evolution," *Tectonics*, vol. 21, no. 1, pp. 6-1–6-17, 2002.

[44] J.-B. Edel, K. Schulmann, and Y. Rotstein, "The Variscan tectonic inheritance of the Upper Rhine Graben: evidence of reactivations in the Lias, Late Eocene–Oligocene up to the recent," *International Journal of Earth Sciences*, vol. 96, pp. 305–325, 2006.

[45] F. Bergerat, *Paléo-champs de contraintes tertiaires dans la plateforme européenne au front de l'orogène alpin*, Bulletin de la Société géologique de France, 1987.

[46] T. Villemin, *Tectonique en extension, fracturation et subsidence: Le Fossé Rhénan et le bassin de Sarre-Nahe*, Doctoral dissertation, 1986.

[47] K. Fuchs, K. Bonjer, D. Gajewski et al., "Crustal evolution of the Rhinegraben area. 1. Exploring the lower crust in the Rhinegraben rift by unified geophysical experiments," *Tectonophysics*, vol. 141, no. 1-3, pp. 261–275, 1987.

[48] T. Villemin and F. Bergerat, *L'évolution structurale du fossé rhénan au cours du Cénozoïque: un bilan de la déformation et des effets thermiques de l'extension*, Bulletin de la Société géologique de France, 1987.

[49] R. Wyns, "Contraintes géologiques et géomorphologiques à l'histoire de la mobilité verticale de la lithosphère continentale en Europe de l'ouest depuis le Crétacé: relations avec la genèse des grabens et du volcanisme tertiaires," in *Colloque "Volcanismes, sédimentations et tectoniques cénozoïques péri-alpins"*pp. 46-47, Doc. BRGM, Aurillac.

[50] C. Sittler, "Illustration de l'histoire géologique du Fossé rhénan et de l'Alsace," *Neues Jahrbuch für Geologie und Paläontologie Abhandlungen*, vol. 186, pp. 255–282, 1992.

[51] J. Vidal, A. Genter, and J. Schmittbuhl, "How do permeable fractures in the Triassic sediments of Northern Alsace characterize the top of hydrothermal convective cells? Evidence from Soultz geothermal boreholes (France)," *Geothermal Energy*, vol. 3, no. 1, 2015.

[52] M. Tesauro, C. Hollenstein, R. Egli, A. Geiger, and H.-G. Kahle, "Continuous GPS and broad-scale deformation across the Rhine Graben and the Alps," *International Journal of Earth Sciences*, vol. 94, no. 4, pp. 525–537, 2005.

[53] A. Genter and H. Traineau, "Borehole EPS-1, Alsace, France: preliminary geological results from granite core analyses for Hot Dry Rock research," *Scientific Drilling*, vol. 2, pp. 205–214, 1992.

[54] C. Dezayes, A. Genter, and B. Valley, "Structure of the low permeable naturally fractured geothermal reservoir at Soultz," *Comptes Rendus Geoscience*, vol. 342, no. 7-8, pp. 517–530, 2010.

[55] J. Stussi, A. Cheilletz, J.-J. Royer, P. Chevremont, and G. Féraud, "The hidden monzogranite of Soultz-sous-Forêts (Rhine Graben, France)," in *Mineralogy, Petrology and Genesis*, vol. 1, pp. 45–64, Géologie de la France, 2002.

[56] G. R. Hooijkaas, A. Genter, and C. Dezayes, "Deep-seated geology of the granite intrusions at the Soultz EGS site based on data from 5km-deep boreholes," *Geothermics*, vol. 35, no. 5-6, pp. 484–506, 2006.

[57] A. Cocherie, C. Guerrot, C. M. Fanning, and A. Genter, "Datation U–Pb des deux faciès du granite de Soultz (Fossé rhénan, France)," *Comptes Rendus Geoscience*, vol. 336, no. 9, pp. 775–787, 2004.

[58] A. Genter, H. Traineau, C. Dezayes et al., "Fracture analysis and reservoir characterization of the granitic basement in the HDR Soultz project (France)," *Geothermal Science and Technique*, vol. 4, pp. 189–214, 1995.

[59] A. Genter, C. Castaing, C. Dezayes, H. Tenzer, H. Traineau, and T. Villemin, "Comparative analysis of direct (core) and indirect (borehole imaging tools) collection of fracture data in the Hot Dry Rock Soultz reservoir (France)," *Journal of Geophysical Research: Solid Earth*, vol. 102, no. B7, pp. 15419–15431, 1997.

[60] A. Genter and H. Traineau, "Analysis of macroscopic fractures in granite in the HDR geothermal well EPS-1, Soultz-sous-Forêts, France," *Journal of Volcanology and Geothermal Research*, vol. 72, no. 1-2, pp. 121–141, 1996.

[61] C. Dezayes, T. Villemin, A. Genter, H. Traineau, and J. Angelier, "Analysis of fractures in boreholes of the Hot Dry Rock project at Soulz-sous-Forêts (Rhine graben, France)," *Scientific Drilling*, vol. 5, pp. 31–41, 1995.

[62] B. Ledésert, J. Dubois, B. Velde, A. Meunier, A. Genter, and A. Badri, "Geometrical and fractal analysis of a three-dimensional hydrothermal vein network in a fractured granite," *Journal of Volcanology and Geothermal Research*, vol. 56, no. 3, pp. 267–280, 1993.

[63] H. Traineau, A. Genter, and J.-P. Cautru, "Petrography of the granite massif from drill cutting analysis and well log

interpretation in the geothermal HDR borehole GPK1 (Soultz, Alsace, France)," *Geothermal Science and Technique*, vol. 3, pp. 1–29, 1991.

[64] B. Ledésert, "Fracturation et Paléocirculations hydrothermales. Application au projet de géothermie roches chaudes sèches de Soultz-sous-Forêts (Alsace)," *Annales de la Société Géologique du Nord*, vol. T4, pp. 13–20, 1995.

[65] B. Ledésert, G. Berger, A. Meunier, A. Genter, and A. Bouchet, "Diagenetic-type reactions related to hydrothermal alteration in the Soultz-sous-Forêts granite, France," *European Journal of Mineralogy*, vol. 11, no. 4, pp. 731–742, 1999.

[66] B. Ledésert, R. Hebert, A. Genter, D. Bartier, N. Clauer, and C. Grall, "Fractures, hydrothermal alterations and permeability in the Soultz Enhanced Geothermal System," *Comptes Rendus Geoscience*, vol. 342, no. 7-8, pp. 607–615, 2010.

[67] M. Dubois, B. Ledésert, J.-L. Potdevin, and S. Vançon, "Détermination des conditions de précipitation des carbonates dans une zone d'altération du granite de Soultz (soubassement du fossé Rhénan, France) : l'enregistrement des inclusions fluides," *Comptes Rendus de l'Académie des Sciences-Series IIA-Earth and Planetary Science*, vol. 331, pp. 303–309, 2000.

[68] B. Ledésert, R. L. Hébert, C. Grall et al., "Calcimetry as a useful tool for a better knowledge of flow pathways in the Soultz-sous-Forêts Enhanced Geothermal System," *Journal of Volcanology and Geothermal Research*, vol. 181, no. 1-2, pp. 106–114, 2009.

[69] M. Dubois, M. Ayt Ougougdal, P. Meere, J.-J. Royer, M.-C. Boiron, and M. Cathelineau, "Temperature of paleo- to modern self-sealing within a continental rift basin: The fluid inclusion data (Soultz-sous-Forêts, Rhine graben, France)," *European Journal of Mineralogy*, vol. 8, no. 5, pp. 1065–1080, 1996.

[70] A. Genter, K. Evans, N. Cuenot, D. Fritsch, and B. Sanjuan, "Contribution of the exploration of deep crystalline fractured reservoir of Soultz to the knowledge of enhanced geothermal systems (EGS)," *Comptes Rendus Geoscience*, vol. 342, no. 7-8, pp. 502–516, 2010.

[71] H. Pauwels, C. Fouillac, and A.-M. Fouillac, "Chemistry and isotopes of deep geothermal saline fluids in the Upper Rhine Graben: origin of compounds and water-rock interactions," *Geochimica et Cosmochimica Acta*, vol. 57, no. 12, pp. 2737–2749, 1993.

[72] P. Durst and F.-D. Vuataz, *Fluid-Rock Interactions in Hot Dry Rock Reservoirs - a Review of the HDR Sites and Detailed Investigations of the Soultz-sous-Forêts System*, World Geothermal Congress, Beppu-Morioka, Japan, 2000.

[73] A. M. Schleicher, L. N. Warr, B. Kober, E. Laverret, and N. Clauer, "Episodic mineralization of hydrothermal illite in the Soultz-sous-Forêts granite (Upper Rhine Graben, France)," *Contributions to Mineralogy and Petrology*, vol. 152, no. 3, pp. 349–364, 2006.

[74] M. P. Smith, V. Savary, B. W. D. Yardley, J. W. Valley, J. J. Royer, and M. Dubois, "The evolution of the deep flow regime at Soultz-sous-Forfts, Rhine Graben, eastern France: Evidence from a composite quartz vein," *Journal of Geophysical Research*, vol. 103, pp. 223–237, 1998.

[75] A. Genter, H. Traineau, B. Ledésert, B. Bourgine, and S. Gentier, *Over 10 Years of Geological Investigations within the HDR Soultz Project, France*, World Geothermal Congress, Kyushu-Tohoku, Japan, 2000.

[76] D. Bartier, B. Ledésert, N. Clauer et al., "Hydrothermal alteration of the Soultz-sous-Forêts granite (hot fractured rock geothermal exchanger) into a tosudite and illite assemblage," *European Journal of Mineralogy*, vol. 20, no. 1, pp. 131–142, 2008.

[77] C. Le Carlier, J. J. Royer, and E. L. Flores, "Convective heat transfer at the Soultz-sous-Forêts Geothermal Site: implications for oil potential," *First Break*, vol. 12, pp. 553–560, 1992.

[78] L. Guillou-Frottier, C. Carrė, B. Bourgine, V. Bouchot, and A. Genter, "Structure of hydrothermal convection in the Upper Rhine Graben as inferred from corrected temperature data and basin-scale numerical models," *Journal of Volcanology and Geothermal Research*, vol. 256, pp. 29–49, 2013.

[79] C. Dezayes and A. Genter, *Large-Scale Fracture Network Based on Soultz Borehole Data*, EHDRA Scientific Conference, Soultz-sous-Forêts, 2008.

[80] S. Haffen, *Caractéristiques géothermiques du réservoir gréseux du Buntsandstein d'Alsace*, Doctoral dissertation, Université de Strasbourg, 2012.

[81] D. J. Marshall, *Cathodoluminescence of Geological Materials*, Taylor & Francis, 1998.

[82] D. K. Richter, T. Götte, J. Götze, and R. D. Neuser, "Progress in application of cathodoluminescence (CL) in sedimentary petrology," *Mineralogy and Petrology*, vol. 79, no. 3-4, pp. 127–166, 2003.

[83] J. Rosenbaum and S. M. F. Sheppard, "An isotopic study of siderites, dolomites and ankerites at high temperatures," *Geochimica et Cosmochimica Acta*, vol. 50, no. 6, pp. 1147–1150, 1986.

[84] C. Pin and C. Bassin, "Evaluation of a strontium specific extraction chromatographic method for isotopic analysis in geological materials," *Analytica Chimica Acta*, vol. 269, no. 2, pp. 249–255, 1992.

[85] J. F. Bauer, S. Meier, and S. L. Philipp, "Architecture, fracture system, mechanical properties and permeability structure of a fault zone in Lower Triassic sandstone, Upper Rhine Graben," *Tectonophysics*, vol. 647-648, pp. 132–145, 2015.

[86] L. Bertrand, J. Jusseaume, Y. Géraud et al., "Structural heritage, reactivation and distribution of fault and fracture network in a rifting context: case study of the western shoulder of the Upper Rhine Graben," *Journal of Structural Geology*, vol. 108, pp. 243–255, 2018.

[87] P. Fluck, J. B. Edel, C. Gagny et al., *Le socle vosgien, segment de la chaine varisque de l'Europe*, vol. 146, Etat des cnnaissances. Propositions d'axes de recherches, 1987.

[88] A. Meunier and B. Velde, "Solid solutions in I/S mixed layer minerals and illite," *American Mineralogist*, vol. 74, pp. 1106–1112, 1989.

[89] S. M. F. Sheppard and H. P. Schwarcz, "Fractionation of carbon and oxygen isotopes and magnesium between coexisting metamorphic calcite and dolomite," *Contributions to Mineralogy and Petrology*, vol. 26, no. 3, pp. 161–198, 1970.

[90] Y. Matsuhisa, J. R. Goldsmith, and R. N. Clayton, "Oxygen isotopic fractionation in the system quartz-albite-anorthite-water," *Geochimica et Cosmochimica Acta*, vol. 43, no. 7, pp. 1131–1140, 1979.

[91] S. I. Golyshey, N. L. Padalko, and S. A. Pechenkin, "Fractionation of stable oxygen and carbon isotopes in carbonate systems," *Geochemistry International*, vol. 18, pp. 85–99, 1981.

[92] J. R. O'Neil, R. N. Clayton, and T. K. Mayeda, "Oxygen isotope fractionation in divalent metal carbonates," *The Journal of Chemical Physics*, vol. 5, pp. 5547–5558, 1969.

[93] J. Horita, "Oxygen and carbon isotope fractionation in the system dolomite-water-CO2 to elevated temperatures," *Geochimica et Cosmochimica Acta*, vol. 129, pp. 111–124, 2014.

[94] Y. Bottinga, "Calculation of fractionation factors for carbon and oxygen isotopic exchange in the system calcite-carbon dioxide-water," *The Journal of Physical Chemistry*, vol. 72, no. 3, pp. 800–808, 1968.

[95] J. G. Blanalt, *Notice et feuille de la carte géologique de Sélestat (307)*, BRGM, Ed., Carte géologique de la France à 1/50 000, 1970.

[96] F. Surma, Y. Geraud, L. Pourcelot et al., "Porosity microstructures of a sandstone affected by a normal fault," *Bulletin de la Societe Geologique de France*, vol. 174, no. 3, pp. 295–303, 2003.

[97] C. Fouillac and A. Genter, *Etude isotopique (O, D, C) des interactions eau-roche dans le granite de Soultz-sous-Forêts, sondage GPK1, site RCS (Alsace)*, BRGM Report R30371/ANA SGN 90, 1990.

[98] M. Cathelineau and M.-C. Boiron, "Downward penetration and mixing of sedimentary brines and dilute hot waters at 5km depth in the granite basement at Soultz-sous-Forêts (Rhine graben, France)," *Comptes Rendus Geoscience*, vol. 342, no. 7-8, pp. 560–565, 2010.

[99] M. Ayt Ougougdal, M. Cathelineau, J. Pironon, M. C. Boiron, D. Banks, and B. W. D. Yardley, *Salt-Rich and Organic-Rich Fluid Migration in the Rhine Graben Triassic Sandstones (Soultz Deep Drilling)*, ECROFI XIII, Sociedad Española de Mineralogia, Sitges, España, 1995.

[100] V. Gardien, M. Rabinowicz, J.-L. Vigneresse, M. Dubois, P. Boulvais, and R. Martini, "Long-lived interaction between hydrothermal and magmatic fluids in the Soultz-sous-Forêts granitic system (Rhine Graben, France)," *Lithos*, vol. 246-247, pp. 110–127, 2016.

[101] M.-C. Boiron, M. Cathelineau, and A. Richard, "Fluid flows and metal deposition near basement/cover unconformity: lessons and analogies from Pb-Zn-F-Ba systems for the understanding of Proterozoic U deposits," *Geofluids*, vol. 10, no. 1-2, 292 pages, 2010.

[102] T. Blaise, J. Barbarand, M. Kars et al., "Reconstruction of low temperature (<100 ˚C) burial in sedimentary basins: a comparison of geothermometer in the intracontinental Paris Basin," *Marine and Petroleum Geology*, vol. 53, pp. 71–87, 2014.

[103] T. Blaise, N. Clauer, M. Cathelineau, M.-C. Boiron, I. Techer, and P. Boulvais, "Reconstructing fluid-flow events in Lower-Triassic sandstones of the eastern Paris Basin by elemental tracing and isotopic dating of nanometric illite crystals," *Geochimica et Cosmochimica Acta*, vol. 176, pp. 157–184, 2016.

[104] A. Genter, N. Cuenot, C. Baujard et al., "Geology, Geophysics and Geochemistry in the Upper Rhine Graben: the frame for geothermal energy use," in *Proceedings of European Geothermal Congress*, pp. 1–5, Strasbourg, France, 2016.

[105] M. Schindler, J. Baumgärtner, T. Gandy et al., "Successful hydraulic stimulation techniques for electric power production in the Upper Rhine Graben, Central Europe," in *Proceedings World geothermal congress*, pp. 1–7, Bali, Indonesia, 2010.

[106] C. Baujard, A. Genter, E. Dalmais et al., "Hydrothermal characterization of wells GRT-1 and GRT-2 in Rittershoffen, France: implications on the understanding of natural flow systems in the rhine graben," *Geothermics*, vol. 65, pp. 255–268, 2017.

[107] P. Herzberger, W. Münch, T. Kölbel et al., "The geothermal power plant Bruchsal," in *Proceedings world geothermal congress*, pp. 1–6, Bali, Indonesia, 2010.

[108] F. Ladner and M. O. Häring, *Hydraulic Characteristics of the Basel 1 Enhanced Geothermal System Hydraulic Reservoir Characterization*, GRC Transactions, 2009.

[109] S. Gentier, X. Rachez, T. D. Tran Ngoc, and C. Souque, "3D flow modelling of the medium-term circulation test performed in the deep geothermal site of Soultz-Sous-forêts (France)," in *World Geothermal Congress 2010*, pp. 25–29, Bali, Indonesia, 2010.

[110] B. Sanjuan, R. Millot, C. Innocent, C. Dezayes, J. Scheiber, and M. Brach, "Major geochemical characteristics of geothermal brines from the Upper Rhine Graben granitic basement with constraints on temperature and circulation," *Chemical Geology*, vol. 428, pp. 27–47, 2016.

[111] B. Sanjuan, R. Millot, C. Dezayes, and M. Brach, "Main characteristics of the deep geothermal brine (5km) at Soultz-sous-Forêts (France) determined using geochemical and tracer test data," *Comptes Rendus Geoscience*, vol. 342, no. 7-8, pp. 546–559, 2010.

[112] C. E. Derer, M. E. Schumacher, and A. Schäfer, "The northern Upper Rhine Graben: basin geometry and early syn-rift tectono-sedimentary evolution," *International Journal of Earth Sciences*, vol. 94, no. 4, pp. 640–656, 2005.

[113] J. P. Brun, M.-A. Gutscher, and dekorp-ecors teams, "Deep crustal structure of the Rhine Graben from dekorp-ecors seismic reflection data: a summary," *Tectonophysics*, vol. 208, no. 1-3, pp. 139–147, 1992.

[114] A. Genter, L. Guillou-Frottier, J. P. Breton et al., *Typologie des systèmes géothermiques HDR/HFR en Europe*, Rapport final BRGM/RP-53452-FR, 2004.

[115] J. F. Vernoux, A. Genter, P. Razin, and C. Vinchon, *Geological and Petrophysical Parameters of a Deep Fractured Sandstone Formation as Applied to Geothermal Exploitation, EPS-1 Borehole*, Rapport BRGM R38622, Soultz-sous-Forêts, France, 1995.

[116] GeORG Team, *Potentiel géologique profound du Fossé Rhénan Supérieur*, Partie 1- Rapport Final BRGM/RP-61945-FR, 2013.

[117] A. Genter, "Géothermie roches chaudes sèches: le granite de Soultz-sous-Forêts (Bas-Rhin, France)," in *Fracturation naturelle, altérations hydrothermales et interactions eau-roche*, p. 201, Thèse Université d'Orléans, 1989.

[118] B. Valley, *The Relation between Natural Fracturing and Stress Heterogeneities in Deep-Seated Crystalline Rocks at Soultz-sous-Forêts (France)*, Doctoral dissertation, ETH Zurich, 2007.

[119] C. Dezayes, C. Lerouge, C. Ramboz, and G. Wille, *Relative Chronology of Deep Circulations within the Fractured Basement of the Upper Rhine Graben*, European Geothermal Congress, Pisa, Italy, 2013.